



**HAL**  
open science

## Recent advances in non-plasmonic SERS nanostructures for biomedical applications

Da Li, Kelly Aubertin, Delphine Onidas, Philippe Nizard, Nordin Felidj, Florence Gazeau, Claire Mangeney, Yun Luo

### ► To cite this version:

Da Li, Kelly Aubertin, Delphine Onidas, Philippe Nizard, Nordin Felidj, et al.. Recent advances in non-plasmonic SERS nanostructures for biomedical applications. Wiley Interdisciplinary Reviews: Nanomedicine and Nanobiotechnology, 2022, 10.1002/wnan.1795 . hal-03685553

**HAL Id: hal-03685553**

**<https://hal.science/hal-03685553>**

Submitted on 2 Jun 2022

**HAL** is a multi-disciplinary open access archive for the deposit and dissemination of scientific research documents, whether they are published or not. The documents may come from teaching and research institutions in France or abroad, or from public or private research centers.

L'archive ouverte pluridisciplinaire **HAL**, est destinée au dépôt et à la diffusion de documents scientifiques de niveau recherche, publiés ou non, émanant des établissements d'enseignement et de recherche français ou étrangers, des laboratoires publics ou privés.

**PLEASE READ ALL 'COMMENT' TEXT BEFORE PREPARING YOUR ARTICLE.** If you do not see the Comments, select View > Print Layout. Please delete the comments (Review > Delete All Comments in Document) and these instructions before submitting so that peer reviewers see a clean copy of the manuscript.

**Remember that you are writing for an interdisciplinary audience.** Please be sure to discuss interdisciplinary themes, issues, debates, etc. where appropriate. Note that the WIREs are forums for review articles, rather than primary literature describing the results of original research.

If you have any questions, [contact your editorial office](#).



Wiley Interdisciplinary Reviews

### Article Title:

**Recent advances in non-plasmonic SERS nanostructures for biomedical applications**

### Article Category:

- PERSPECTIVE       PRIMER       OVERVIEW  
 ADVANCED REVIEW       FOCUS ARTICLE       SOFTWARE FOCUS

### Authors:

<b>First author full name</b>
Da Li
LCBPT, CNRS UMR 8601, Université de Paris. 45, rue des Saints-Pères, 75006 Paris, France.
Email : <a href="mailto:da.li@etu.u-paris.fr">da.li@etu.u-paris.fr</a>
<b>Second author full name</b>
Kelly Aubertin
MSC, CNRS UMR 7057, Université de Paris. 45, rue des Saints-Pères, 75006 Paris, France.
Email : <a href="mailto:kelly.aubertin@univ-paris-diderot.fr">kelly.aubertin@univ-paris-diderot.fr</a>
<b>Third author full name</b>
Delphine Onidas

LCBPT, CNRS UMR 8601, Université de Paris. 45, rue des Saints-Pères, 75006 Paris, France.

Email : [delphine.onidas@parisdescartes.fr](mailto:delphine.onidas@parisdescartes.fr)

**Fourth author full name**

Philippe Nizard

LCBPT, CNRS UMR 8601, Université de Paris. 45, rue des Saints-Pères, 75006 Paris, France.

Email : [philippe.nizard@parisdescartes.fr](mailto:philippe.nizard@parisdescartes.fr)

**Fifth author full name**

Nordin Félidj

ITODYS, CNRS UMR 7086, Université de Paris. 15, rue Jean Antoine de Baïf, 75013 Paris, France.

Email : [nordin.felidj@univ-paris-diderot.fr](mailto:nordin.felidj@univ-paris-diderot.fr)

**Sixth author full name**

Florence Gazeau

MSC, CNRS UMR 7057, Université de Paris. 45, rue des Saints-Pères, 75006 Paris, France.

Email : [florence.gazeau@univ-paris-diderot.fr](mailto:florence.gazeau@univ-paris-diderot.fr)

**Seventh author full name**

Claire Mangeney

LCBPT, CNRS UMR 8601, Université de Paris. 45, rue des Saints-Pères, 75006 Paris, France.

Email : [claire.mangeney@parisdescartes.fr](mailto:claire.mangeney@parisdescartes.fr)

**Corresponding author full name**

Yun Luo

LCBPT, CNRS UMR 8601, Université de Paris. 45, rue des Saints-Pères, 75006 Paris, France.

Email : [yun.luo@u-paris.fr](mailto:yun.luo@u-paris.fr)

ORCID iD: 0000-0002-9515-0460

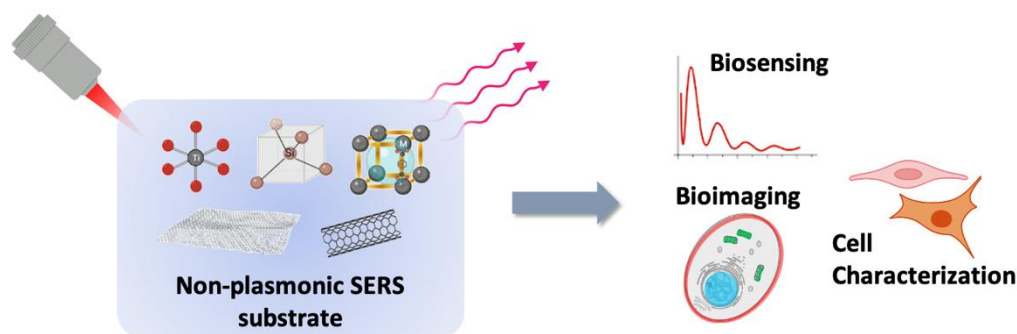
## Conflict of Interest

The authors declare that they have no known competing financial interests or personal relationships that could have appeared to influence the work reported in this paper.

## Abstract

Surface-enhanced Raman spectroscopy (SERS) is an emerging powerful vibrational technique offering unprecedented opportunities in biomedical science for the sensitive detection of biomarkers and the imaging and tracking of biological samples. Conventional SERS detection is based on the use of plasmonic substrates (e.g. Au and Ag nanostructures), which exhibit very high enhancement factors ( $EF = 10^{10}$ - $10^{11}$ ) but suffers from serious limitations, including light-induced local heating effect due to ohmic loss and expensive price. These drawbacks may limit detection accuracy and large-scaled practical applications. In this review, we focus on alternative approaches based on plasmon-free SERS detection on low-cost nanostructures, such as carbons, oxides, chalcogenides, polymers, silicons, *etc.* The mechanism of non-plasmonic SERS detection has been attributed to interfacial charge transfer between the substrate and the adsorbed molecules, with no photothermal side effects but usually less EF compared with plasmonic nanostructures. The strategies to improve Raman signal detection, through the tailoring of substrate composition, structure and surface chemistry, is reviewed and discussed. The biomedical applications, e.g. SERS cell characterization, biosensing and bioimaging are also presented, highlighting the importance of substrate surface functionalization to achieve sensitive, accurate analysis and excellent biocompatibility.

## Graphical/Visual Abstract and Caption



**Non-plasmonic SERS detection for biomedical applications.**

## 1. INTRODUCTION

Raman spectroscopy is attracting growing attention in biomedical science in view of its potential for the sensing of biomarkers, the imaging of cells and tissues and the tracking of biological processes.<sup>1</sup> The Raman effect, based on the inelastic scattering of light from samples under irradiation, allows us to probe the vibrational states of molecules and materials, thus providing rich spectral fingerprints of various types of analytes. Moreover, as water is a weak Raman scatterer, this non-destructive technique offers added-value for biomedical diagnosis and tissue imaging compared to infrared spectroscopy which is highly sensitive to water.<sup>2</sup> However, most photons undergo elastic scattering (called Rayleigh scattering) and only a few photons (one over  $10^6$ ) contribute to the Raman process.<sup>3</sup> As a result, Raman signals are very weak which strongly limits the interest of this technique for many applications. In order to improve the signal intensities, several enhanced Raman spectroscopic methods have been explored, from stimulated or coherent anti-Stokes Raman scattering to surface-enhanced Raman scattering. In this review, we will focus exclusively on surface-enhanced Raman spectroscopy (SERS) approaches, which allow to increase the sensitivity of Raman spectroscopy by several orders of magnitude. It takes advantage of the local field enhancement offered by optically resonant metal nanoparticles (NPs) to amplify Raman signals and leads to high-sensitivity label-free identification of molecular species.<sup>4</sup> It thus combines the rich molecular information contained in vibrational spectra with outstanding ultra-sensitive, multiplexing, and quantification capabilities. The increase of Raman signal intensities observed in SERS has been explained by two main mechanisms: (i) an electromagnetic enhancement due to the concentration of the local electric field by surface plasmons in the vicinity of nanostructured metal surfaces; (ii) a chemical enhancement through a charge transfer process between the analytes and the metal surface. The former mechanism can only be achieved on plasmonic substrates, such as noble metal nanomaterials<sup>5</sup> while the latter one can be obtained on both plasmonic and plasmon-free materials.

Although the enhancement factors (EF) reached on plasmonic substrates are very high, typically in the range  $10^{10}$ - $10^{11}$ , allowing single molecule detection,<sup>6</sup> the biosafety of plasmonic NPs is still a great issue. Thus surface modification is usually necessary to improve their biocompatibility.<sup>7</sup> Moreover, the high price of noble metals such as Au and Ag hinders their large-scale application in the biomedical field. Compared to their plasmonic counterparts, the EF of plasmon-free substrates are much lower with values ranging from  $10^2$  to  $10^5$ .<sup>8, 9</sup> Yet, these materials, based on carbon, silicon, oxides,

chalcogenides, *etc.* could be a low-cost alternative as SERS substrates. In this review, we will focus on this promising class of SERS substrates, based on non-plasmonic materials, introducing the fundamental aspects of chemical enhancement mechanism (CM), the various synthesis methods and categories of materials and their practical applications in biomedical fields (Figure. 1).

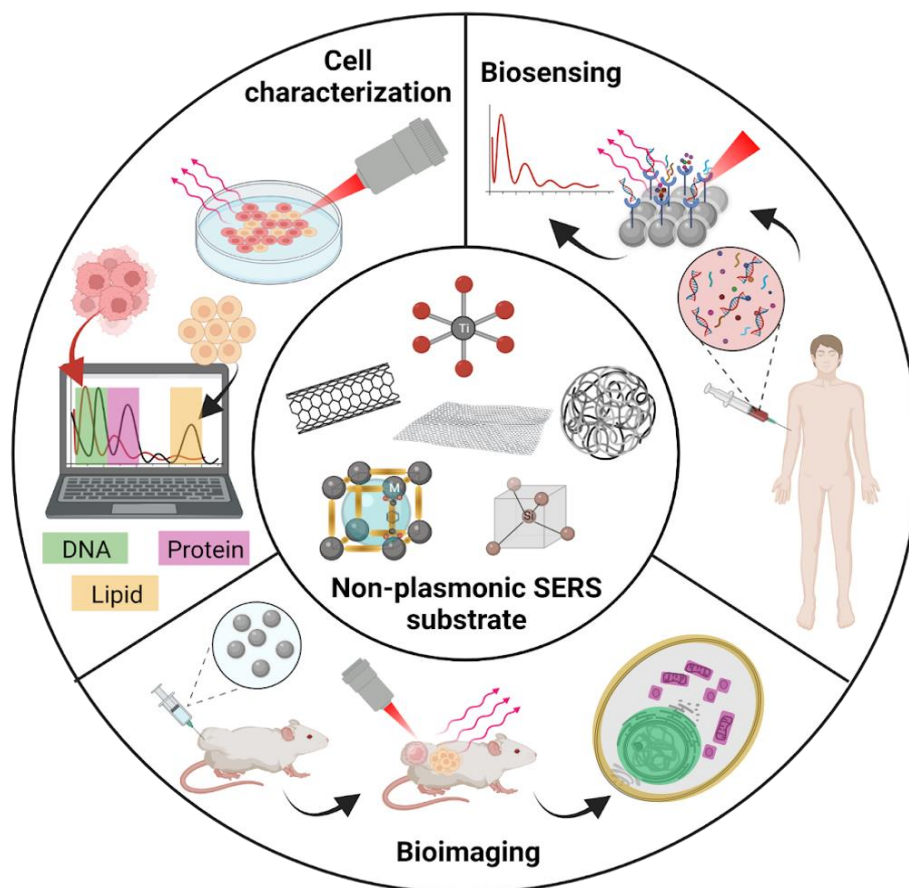


**Figure 1.** Illustration of nanomaterials (carbon nanotubes, graphenes, carbon 3D networks, TiO<sub>2</sub>, Si and metal-organic frameworks, etc...) for non-plasmonic SERS biomedical applications (e.g. biosensing, bioimaging and cell characterization). Created by BioRender.

## 2. FUNDAMENTAL ASPECTS: FROM SPONTANEOUS RAMAN TO SERS

### 2.1 Spontaneous Raman

If a material is illuminated with an intense monochromatic radiation of frequency  $\nu_0$  from a laser source, the photons constituting this radiation can be transmitted, absorbed or scattered in all the directions of space. Spectroscopic analysis of the scattered light shows that most of the re-emitted photons have the same frequency  $\nu_0$  as the incident radiation. This scattering without changing frequency is called Rayleigh scattering (or elastic scattering). For less than a million scattered photons, a change in frequency can be observed: this inelastic scattering of light constitutes the

Raman effect. As the spontaneous Raman process is generally not very efficient, it is essential to eliminate the Rayleigh scattering, the main component of scattered light, by using a monochromator or filters (edge or notch). The frequencies of the inelastically scattered photons are  $\nu_{RS} = \nu_0 - \nu_V$  and  $\nu_{RAS} = \nu_0 + \nu_V$ , where  $\nu_V$  is the frequency of a mode of vibration while  $\nu_{RS}$  and  $\nu_{RAS}$  represent the frequencies of the Stokes and anti-Stokes Raman scattering, respectively. From a microscopic point of view, the Raman effect stems from the appearance of an induced dipole moment linked to the polarizability of molecules, namely, the capability of the electron cloud of a molecular system to deform under the effect of an electric field. In the context of a quantum description, it can be shown that the ratio of the Raman Stokes and anti-Stokes intensities is proportional to the ratio of the populations of the vibrational levels, which obeys Boltzmann law. As a consequence, the Stokes intensity is systematically greater than the anti-Stokes one, and the ratio of these intensities gives access to the temperature of the medium probed by the Raman effect. Interestingly, if the incident laser excitation wavelength corresponds to the energy required for an electronic transition in the molecule, the Raman scattering is strongly enhanced (gain from  $10^3$  to  $10^4$ ), which is called resonant Raman effect.

## **2.2 SERS: plasmon versus non-plasmon enhancement**

As explained in the previous paragraph, classical (or spontaneous) Raman spectroscopy is a very insensitive technique, which limits the analysis of low concentration products. However, the adsorption of molecules on the surface of nanostructures (mainly gold and silver), makes it possible to enhance their Raman signature, even at very low concentrations, which is called surface enhanced Raman scattering.<sup>10</sup> The SERS effect can be attributed to physical or/and chemical mechanisms, as shown in Figure. 2. Physical phenomenon induced by localized surface plasmon resonance is known as electromagnetic enhancement mechanism (EM). The chemical enhancement mechanism (CM) based on charge transfer between substrate and surface adsorbed molecule can also induce SERS. It is worth noting that fluorescence quenching and birefringence effects could also help to improve Raman signals detection, but these effects should be distinguished from EM- and CM-induced SERS. In this section, we will discuss both plasmonic and non-plasmonic SERS effects, introducing the different mechanisms and comparing their limitations and merits.

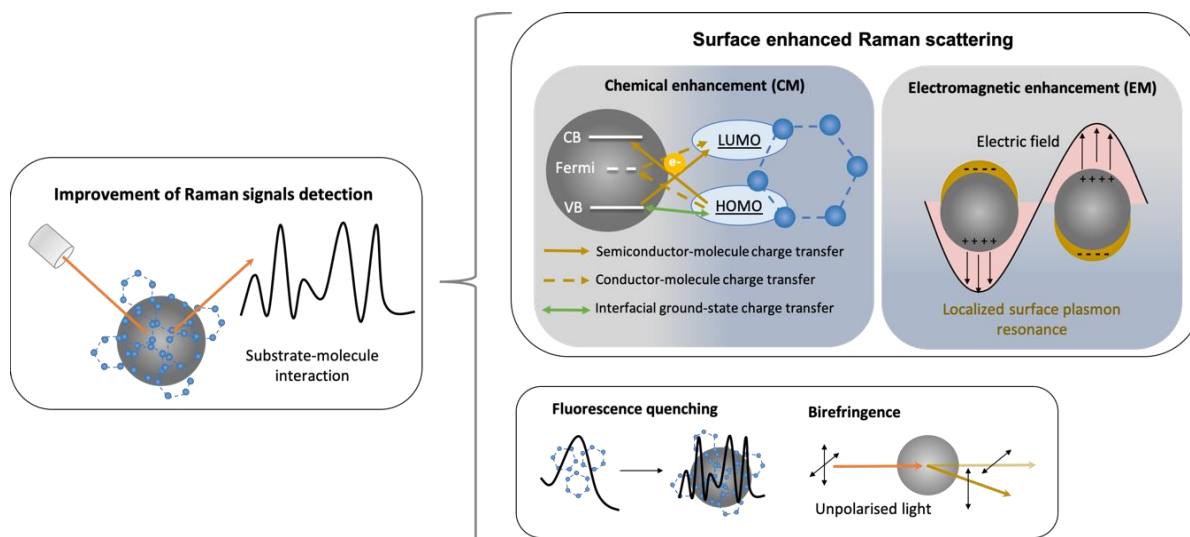


**Figure 2.** Illustration of Raman signal enhancement mechanisms, based on (EM) electromagnetic field interacting with a metal sphere; (CM) electron transfer between a particle and a molecular adsorbate (yellow and green arrows); (Fluorescence quenching) illustration of the quenching of fluorescence process: formation of an adsorbate/metal complex resulting in an additional channel of nonradiative return to ground state; (birefringence) in chiral substrates.

**Plasmonic SERS (EM mechanism).** This effect occurs when molecules are adsorbed on metallic nanostructures such as rough surface, colloidal nanoparticles or self-assembled and lithographic metal particles. The enhancement of the Raman spectra can reach a factor of the order of  $10^{10}$ - $10^{11}$ .<sup>6, 11</sup> The first observations of a surface-enhanced Raman spectrum were made in the mid-1970s in the case of pyridine adsorbed on the surface of a silver electrode roughened by redox cycles, or in aggregated colloidal dispersions of silver nanoparticles.<sup>12</sup> As shown in Figure. 2, the origin of the SERS effect is attributed to the amplification of the local electric field, following the excitation of localized surface plasmons (LSP). This optical phenomenon corresponds to a collective phase oscillation of the conduction electrons at the surface of the nanostructure, under light excitation.<sup>13</sup> It leads to strong extinction bands in the visible and near-infrared spectral range (in particular for gold and silver), whose wavelengths depend on the nanoparticle size, shape, and the local dielectric environment.<sup>14</sup> These oscillations also result in a strong amplification of the local field in the vicinity of the nanostructures, affecting the induced dipole moment of adsorbed molecules.<sup>15, 16</sup>

**Non-plasmonic SERS (CM mechanism).** In addition, a chemical effect might contribute to the SERS effect. As shown in Figure. 2, this chemical enhancement involves changes of the adsorbate electronic states due to the chemisorption of the analyte. An increase in the polarizability of the

molecule during its interaction with the substrate surface (such as carbon, oxides and so on, which is discussed in section 3) may take place, but the associated enhancement factor is usually lower than that of their plasmonic counterparts.<sup>17</sup> The origin of CM is still under study, but various types of charge transfer (CT) process have been reported to enhance Raman signals under appropriate laser excitation. For example, CT can take place between the Fermi level of conducting substrate and the highest occupied molecular orbital or the lowest unoccupied molecular orbital (HOMO or LUMO), cf. dash yellow arrows of CM in Figure. 2. It occurs also between valence/conducting band (VB/CB) in semiconducting materials and HOMO/LUMO (solid yellow arrows of CM in Figure. 2). Recently, conductive polymers have been explored for non-plasmonic SERS where the CT happens between molecular orbitals (HOMO/LUMO) of adsorbate and substrate.<sup>18</sup> In addition to the SERS effects induced by substrate-molecule interfacial CT, Raman resonance effects obtained *via* molecule HOMO to LUMO transitions or exciton transitions between VB and CB of semiconductors could also take place, resulting in Raman signal enhancement.<sup>19</sup> Besides, interfacial solid-states CT caused by chemisorption of molecules on substrate, e.g. formation of metal-molecule complexes without excitation, might also be responsible for CM (green arrow, CM in Figure. 2).

**Besides EM and CM.** Another aspect to improve Raman signals is the quenching of fluorescence of the adsorbates. Auto-fluorescence of the analyte is considered as an intense background which strongly interferes with the detection of Raman signal. Therefore, the suppression of fluorescence is important and necessary. The fluorescence quenching effect can be observed on plasmonic NPs surface (e.g. Au) due to resonant energy transfer.<sup>20, 21</sup> The formation of an adsorbate/metal complex results in an additional channel of nonradiative return to the ground state.<sup>22</sup> This phenomenon has also been reported on non-plasmonic substrates, such as nanostructured carbon surfaces.<sup>23</sup> Recently, laser-driven birefringence has been reported for SERS.<sup>24, 25</sup> As described in these works, birefringence generated under laser irradiation in nanofibers could induce multiple Raman scattering, resulting in plasmon-free SERS activity. The fundamental aspects for SERS effect based on birefringence is still unclear.

### **2.3 Merits and drawbacks of plasmonic NPs**

SERS benefits from a strong amplification of the local electric field in the vicinity of the nanostructures and the related enhancement of the Raman spectra of molecules adsorbed on the nanostructure surface. The main advantages of SERS, using plasmonic NPs, include a high level of multiplexing, the ability to perform the detection of compounds at very low concentration in complex media such as in blood or urines. SERS is also a non-destructive and a label-free technique. Although plasmonic particles achieve a Raman gain around  $10^{10}$ - $10^{11}$ ,<sup>6</sup> their major disadvantage is a significant temperature rise of the structure, resulting from strong light absorption by the metals. Indeed, some losses arising from interband transitions when a valence electron in the metal absorbs a photon to jump to the Fermi surface.<sup>26</sup> This loss effect leads to Joule heating of the particle within the local environment.<sup>27</sup> This greatly limits their use for studies of biological systems, very sensitive to temperature changes. Unlike metals, dielectric structures have very low absorption cross-sections (and thus low thermal conversion) and relatively intense scattering spectra. Besides, plasmonic SERS are usually achieved on noble metals, e.g. Au and Ag nanostructures. So, the costs are usually expensive, which limits the large-scale application of SERS in the biomedical domain.

### **2.4 New opportunities offered by non-plasmonic NPs**

The appeal of dielectric nanostructures for SERS was recently demonstrated with Raman gains of the order of  $10^3$  from dimers of silicon nanostructures.<sup>28</sup> Interestingly, dielectric nanoparticles generate heating effects with temperature increase values equal to 1/18 times that of Au plasmon-analogue systems, while Au NPs only double the field enhancement capability compared to the dielectric ones. Therefore, non-plasmonic nanoparticles appear as a very promising alternative for surface-enhanced spectroscopies in the context of vibrational characterization of biological systems, with the particularity of not perturbing the signal of the target analyte or biomarker by undesired local heating.

## **3. NON-PLASMONIC SUBSTRATES**

A wide range of plasmon-free substrates for SERS have been described in the literature. In this section, we summarize the various nanostructures, including carbon-based materials, oxides, chalcogenides, silicon and polymers. Their nature and morphology are described as well as the SERS mechanisms and corresponding enhancement factors.

### 3.1 Carbon-based materials

Carbon-based nanomaterials have been reported as SERS substrates for chemical/biological sensing, analyte identification and bioimaging.<sup>29-31</sup> Compared with metallic SERS substrates (e.g. Au or Ag NPs), carbon is abundant, recyclable, environment-friendly and gives low-cost materials. Carbon nanomaterials are usually used as templates to fabricate metal NPs (ex. Au, Ag) or as supports to load the NPs which act as Raman nano-amplifiers of absorbed molecules.<sup>32-34</sup> In this case, the EM from metal NPs mainly contributes to the SERS phenomenon in hybrid metal-carbon nanocomposites. Without metal NPs, LSP can be also generated on sole carbon surface by ultra-violet (UV) irradiation, which induces  $\pi$ -plasmon absorption (collective oscillations of  $\pi$  electrons originated from the graphite structure).<sup>35, 36</sup> The LSP band of carbon, namely, collective oscillations of long-lived electrons, is located the in terahertz or/and infrared (IR) region.<sup>37, 38</sup> Therefore, it is unlikely that the EM is responsible for SERS effect observed on sole carbon materials under visible light excitation. Instead, it should be attributed to chemical enhancement (CM) originating from charge transfer between carbon and surface immobilized molecules. Besides, for chiral carbon nanostructures (chiral carbon nanotubes), optical Kerr effect induced birefringence could also amplify the Raman signal of surface adsorbed molecules.<sup>24</sup> In this section, we will introduce different types of carbon substrates for plasmon-free SERS detection, including zero dimensional (D), 1D, 2D, 3D carbon nanomaterials.

**0D graphene quantum dots (GQDs).** GQDs refer to graphene fragments smaller than 100 nm,<sup>39</sup> which possess unique optoelectronic properties (photoluminescence and non-zero bandgap) due to quantum confinement.<sup>40</sup> GQDs have been widely applied as fluorescent agents for bioimaging.<sup>41</sup> Regarding SERS, it is worth to note that, theoretical calculation showed that GQDs have similar surface plasmon frequencies as metal NPs,<sup>42</sup> so that, EM could take place also on GQDs under visible incident light. However, experimentally, the synthesized GQDs present defects, so the plasmon band frequency shifts out of visible range. Therefore, the CM should be responsible for observed SERS effects.<sup>43, 44</sup> Recently, *Lan et al* reported a nanocomposite derived from GQDs and  $\text{Mn}_3\text{O}_4$ <sup>43</sup> for cancer cell characterization. In this work, self-assembled GQDs- $\text{Mn}_3\text{O}_4$  nanocomposite has been prepared from multi-walled carbon nanotubes (CNTs) by  $\text{KMnO}_4$  oxidative cut (Figure 3a). The oxide could quench GQDs' fluorescence due to a charge transfer in the nanocomposite. It could

also suppress the fluorescence of adsorbed molecules (e.g. rhodamine B, RhB), as shown in Figure 3b and Table 1, which significantly improves Raman signal. The enhancement factor (EF) was  $2.06 \times 10^4$  for RhB. As shown in the energy level diagram (Figure 3c), charge transfers from VB to LUMO ( $\mu_{CT}$ , ca. 2.41 eV) and HOMO to CB (ca. 1.11 eV) are allowed under 514 nm (2.4 eV) laser excitation. The former is known as C-term charge transfer (VB  $\rightarrow$  LUMO), which has been identified as the main contribution for SERS effect induced by CM, compared with A-term ( $\mu_{mol}$ , HOMO  $\rightarrow$  LUMO), B-term ( $\mu_{CT}$ , HOMO  $\rightarrow$  CB) and VB  $\rightarrow$  CB ( $\mu_{ex}$ ) transitions.<sup>19</sup> The GQDs-Mn<sub>3</sub>O<sub>4</sub> nanocomposites were used as a SERS substrate for cancer cell identification. As shown in Figure 3d, distinctive SERS spectra could be obtained for cancer (HeLa, HepG-2) and normal (7702) cells on GQDs-Mn<sub>3</sub>O<sub>4</sub>. Another example was nitrogen-doped GQDs (N-GQDs), synthesized via solvothermal route (a modified Hummers' method) using graphene oxide as precursor and N,N-Dimethylformamide as nitrogen source and solvent.<sup>44</sup> After adsorption of RhB, N-GQDs exhibited SERS effect with an EF of  $3.2 \times 10^3$  (at  $10^{-4}$  M of RhB) and a limit of detection (LOD) of  $10^{-10}$  M due to substrate-molecule charge transfer process under 488 nm excitation (Table 1).

**1D carbon nanotubes (CNTs).** CNTs are defined as cylindrical graphite with high aspect ratio (diameter *versus* length), which can be considered as 1D structures in electronic point of view.<sup>45</sup> In most cases, CNTs are applied as templates or supports for metal NPs to generate hybrid plasmonic SERS substrates.<sup>34</sup> However, it is possible to fabricate substrates for non-plasmonic Raman detection. For example, *Qiu* and co-workers have reported TiO<sub>2</sub> decorated chiral CNTs (R/L-CNTs/TiO<sub>2</sub>) as a recyclable platform for plasmon-free SERS detection.<sup>24</sup> Such hybrid nanocomposites (Figure 3e) were prepared via carbonization of chiral polypyrrole nanotubes, followed by TiO<sub>2</sub> NPs deposition. The chiral CNTs exhibit improved SERS sensitivity for surface adsorbed methylene blue (MB) molecules under 532 nm laser excitation, due to birefringence induced by optical Kerr effect on chiral structures,<sup>46</sup> as shown in Figure 3f. As listed in Table 1, the LOD for such a system is  $5 \times 10^{-5}$  M. After long-term irradiation, photo-degradation of MB took place on TiO<sub>2</sub> NPs, leading to a self-cleaning process (Figure 3g).

**2D graphene sheets.** Graphene is a 2D graphite film, composed of sp<sup>2</sup> carbon atoms tightly bound in a hexagonal honeycomb lattice.<sup>47</sup> In the domain of plasmon-free SERS, graphene enhanced Raman scattering (GRES), has been proven as the result of charge transfer between graphene and

target molecules.<sup>48</sup> The quantitative analysis based on GERS is still a great challenge because lots of parameters (ex. adsorbed molecule orientation and layer thickness, Fermi level, doping states, etc.) affect GERS efficiency. Nevertheless, some works achieved GERS biosensing by deposition of graphene on oxide support. For example, *Zheng et al* reported a graphene-TiO<sub>2</sub> (EG-TiO<sub>2</sub>) SERS substrate to track telomerase activity of stem cells.<sup>49</sup> In this work, 2D graphene was electrodeposited onto TiO<sub>2</sub> nanoarrays (Figure 3h), followed by immobilization of primer-DNA. This results in a 3D nanocomposite, displaying specific recognition of telomerase. In presence of probing copper phthalocyanine (CuPC), G-quadruplex could be formed on EG-TiO<sub>2</sub> (Figure 3i). Thanks to the semiconducting TiO<sub>2</sub>, the Fermi level of EG (ca. -4.6 eV) could be shifted to a higher level (EG-TiO<sub>2</sub>, ca. -3.65 eV) due to Schottky junction (Figure 3j). This value is closer to LUMO (ca. -3.07 eV) of CuPC, leading to easier charge transfer and thus stronger Raman signals under 633 nm (ca. 1.96 eV) with EF = 48.2 rather than 532 nm laser exposition (EF = 39.2), cf. Table 1. As the LOD of CuPC could be as low as  $6 \times 10^{-5}$  M (ca.  $2.07 \times 10^{-16}$  IU), EG-TiO<sub>2</sub> was thus used for tracking telomerase activity in stem cells (Figure 3k), which further reveals that telomerase plays an important role in proliferation and differentiation of stem cells. In another work, reported by *Huang et al*, the graphene was used as a SERS substrate for label-free analysis of key blood constituent proteins.<sup>50</sup> The graphene flakes were synthesized by mechanical exfoliation and placed on Si/SiO<sub>2</sub> support. Two proteins, namely hemoglobin and albumin, could be detected on graphene surface due to the GERS effect, offering a new strategy to develop reliable, simple and molecular fingerprinting biosensing techniques for blood samples. The EF for hemoglobin was about 4.5 under 633 nm laser (Table 1). Beside oxides, semiconducting sulfites could also serve as a platform to load graphene. For example, MoS<sub>2</sub> sheet decorated graphene microflowers (GMFs/W-MoS<sub>2</sub>) have been used for plasmon-free SERS enhancement<sup>51</sup> with EF as high as  $2.96 \times 10^7$  and LOD of  $5 \times 10^{-11}$  M for RhB under 633 nm laser. As a proof-of-concept, such a substrate has been used for adenosine sensing, where the detection limit was as low as  $2 \times 10^{-9}$  M. This shows great potential of GMFs/W-MoS<sub>2</sub> in biosensing.

**3D carbon nanostructures** are built by spatial assembly of 0D carbon quantum dots, 1D CNTs or 2D graphene.<sup>9, 52</sup> Non-plasmonic SERS biosensing can be also realized by 3D interconnected nanocarbon web (INW).<sup>9</sup> Such a structure was created on a graphite plate (3 mm thickness) by ultrashort laser ablation. The morphology and composition (ratio of C-O and C-C bonds) of INW could

be controlled by ionization energy (Figure 3l). The SERS effect was confirmed using crystal violet and R6G dye molecules, induced by charge transfer resonance in the interface of INW and dye molecules. The EF value was calculated as  $3.66 \times 10^4$  and  $9.1 \times 10^3$  respectively using crystal violet and R6G dye under 785 nm laser (Table 1). The INW was later incubated with HeLa and fibroblast cells for 6, 12, 18 and 24h. The distinctive SERS spectra can be respectively acquired on cancerous and normal cells (Figure 3m). One could observe the dissimilar Raman peak evolution of different intracellular components, as summarized in Figure 3n. Therefore, the INW could serve as a SERS platform to *in vitro* probe and differentiate cancerous and normal cells.

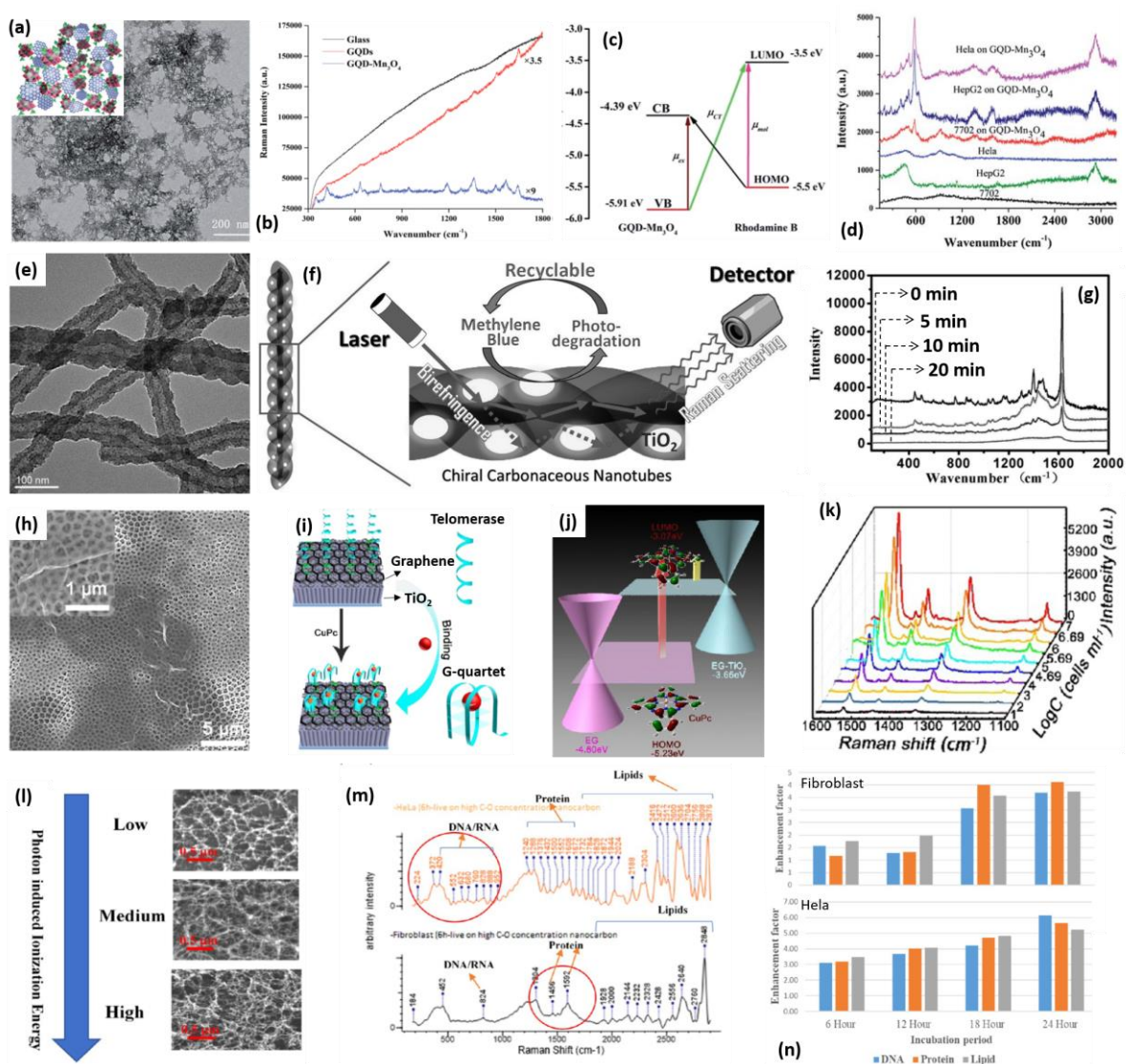


**Figure 3.** (a) TEM and (inset) illustrative image of GQDs-Mn<sub>3</sub>O<sub>4</sub> nanocomposites. (b) Raman spectra of RhB on glass, GQDs and GQDs-Mn<sub>3</sub>O<sub>4</sub>. (c) Energy level diagram for GQDs-Mn<sub>3</sub>O<sub>4</sub> and RhB molecule. (d) Raman spectra of HeLa, HepG2 and 7702 cells on SERS active GQDs-Mn<sub>3</sub>O<sub>4</sub> substrate and glass slip. Reproduced (Adapted) with permission from Ref. 43, Copyright 2017, Royal Society of Chemistry. (e) TEM image of chiral R-

CNTs/TiO<sub>2</sub>. (f) Proposed mechanism of recyclable SERS substrate based on chiral CNTs/TiO<sub>2</sub>. (g) The evolution of SERS spectra for MB molecules onto R-CNTs/TiO<sub>2</sub> during simulated solar light irradiation of 20 min. Reproduced (Adapted) with permission from Ref. 24, Copyright 2015, Wiley. (h) SEM image (inset top view) of EG-TiO<sub>2</sub>. (i) Scheme of sensing principle of telomerase in presence of CuPC on surface modified EG-TiO<sub>2</sub>. (j) Scheme of SERS mechanism of CuPC onto EG-TiO<sub>2</sub>. (k) SERS spectra obtained with stem cell concentrations of 10, 10<sup>2</sup>, 10<sup>3</sup>, 10<sup>4</sup>, 10<sup>5</sup>, 10<sup>6</sup>, and 10<sup>7</sup> cells mL<sup>-1</sup>. Reproduced (Adapted) with permission from Ref. 49, Copyright 2017, American Chemical Society. (l) SEM images of INWs obtained with low, medium and high ionization energy. (m) SERS spectra and Raman peak assignments for live HeLa (top) and fibroblast (bottom) cells incubated with INWs for 6h. (n) Summary of Raman peak evolution for live HeLa and fibroblast cells incubated with INWs for 6, 12, 18 and 24h. Reproduced (Adapted) with permission from Ref. 9, Copyright 2018, American Chemical Society.

### 3.2. Metal oxide-based SERS substrates

Semiconducting oxides NPs (ZnO, TiO<sub>2</sub>, SiO<sub>2</sub>, Cu<sub>2</sub>O and Fe<sub>3</sub>O<sub>4</sub> NPs) are one of the most studied non-plasmonic SERS substrates due to their engineerable band gap, tunable morphology and modifiable surface.<sup>53-61</sup> The engineerable band gap, through composition altering such as doping, alloying, superlattice,<sup>62</sup> allows adaptable charge transfer in oxide-molecule interface and favors sensitive analysis *in vivo* or *in vitro*. It is well known that NPs morphology (size and shape) as well as surface plays an important role in biological processes.<sup>63</sup> The tunable morphology and functionalized surface help SERS NPs to follow specific reactions with controlled cytotoxicity. In addition, recent research has found an SERS effect related to surface defects.<sup>64</sup> It is worth noting that non-plasmonic SERS efficiency could be affected by size of oxides, which should be attributed to size-dependent surface defects or band-gap energy level.<sup>65, 66</sup> Therefore, in this section, we have summarized the latest research on oxides SERS substrates, focusing on their structure, morphology impacted SERS mechanism and performance.

**ZnO** particles or substrates showed promising potentials for SERS, particularly for bioapplications thanks to the low cytotoxicity of this material.<sup>67, 68</sup> The poor stability of ZnO in water may be overcome with a coating made of triethylene glycol and oleic acid, able to penetrate cells.<sup>68</sup> ZnO substrate was found to enhance the signal of molecules such as 4-mercaptopyridine and 4-mercaptobenzoic acid.<sup>19</sup> An increased enhancement factor, as high as 10<sup>5</sup> (Table 1) was also found in amorphous nanocages promoting an interfacial charge transfer process due to metastable electronic states.<sup>53</sup> Besides, *Haldavnekar et al.* found that the enhancement factor was even higher as the particles were smaller, by talking about optimal ZnO quantum probe size in the range of 5.7 - 8.1 nm.<sup>54</sup> These nanoparticles

exhibited high surface area, good crystallinity, sensitivity due to a wide band gap, and biocompatibility. SERS effect was observed at different excitation wavelengths with a higher efficiency at 785 nm ( $EF = \sim 10^6$ ,  $LOD = 10^{-9}$  M, cf. Table 1) and smaller at 532 nm or 638 nm. The enhancement was explained by 3 co-existent mechanisms: (i) charge transfer resonance, (ii) photo-induced charge transfer from attenuated total reflection causing near field interaction due to quantum size, (iii) and surface plasmon resonance (induced by 785 nm excitation) in a unified molecule–semiconductor quantum probe system. Such a synergy was shown to boost the SERS probe sensing sensitivity. In this work, the authors used ingenious nano-dendrite platforms decorated with ZnO quantum probes allowing cell adhesion for effective enhancement of Raman signal of biomolecules, which could be applied for cancer and normal cell differentiation (Figure 4a).

**TiO<sub>2</sub>.** Although TiO<sub>2</sub> may be less biocompatible due to its cytotoxicity, its low cost, high adsorptivity and chemical stability make it nevertheless a good candidate for non-plasmonic SERS material, which have shown some potential for bioapplications like the diagnosis of breast cancer.<sup>55</sup> In this paper, the authors used quantum-structured TiO<sub>2</sub> (1-10 nm) or quantum-structured TiO<sub>x</sub> (noted as Q-structured TiO<sub>x</sub>, cf. TEM in Figure 4b) in which they introduced oxygen vacancies (confirmed by X-ray photoemission spectroscopy, see O 1s spectra in Figure 4b), allowing to gain 2 orders of magnitude on the enhancement factor reaching  $3.4 \times 10^7$  with a LOD value of  $10^{-9}$  M for crystal violet molecules, as summarized in Table 1. Such a nanotool has been applied as a SERS probe to distinguish normal and cancerous cells (Figure 4b). A similar technique of introducing oxygen defects increasing charge transfer yield in the subsurface of a quantum probe was developed by *Dharmalingam et al.* TiO<sub>2</sub> nanoparticles were deposited on Ti substrate and oxygen defects were induced with multiphoton ionization. This technique allows them to increase the sensitivity of the semiconductor and to reach an EF of  $10^{10}$  and LOD of  $10^{-9}$  M for crystal violet thanks to the synergistic effect of the quantum size and the high charge-transfer called atomic-defect enhanced Raman scattering.<sup>56</sup> Another strategy to improve SERS activity is based on tailoring TiO<sub>2</sub> morphology. For example, as shown in Figure 4c, crystal-amorphous core-shell TiO<sub>2</sub> NPs have been prepared,<sup>57</sup> showing EF as high as  $4.3 \times 10^5$  and LOD of  $5 \times 10^{-4}$  M for 4-nitrobenzethiol (Table 1). Such a structure leads to core-shell heterojunction, favoring separation and injection of exciton (generated in the core) into the shell. This leads to a charge enriched shell, easily undergoing substrate-molecule charge transfer (Figure 4c).

After surface functionalization of Raman tag and bioreceptor, it could be used for cancer cell Raman imaging (Figure 4c). Besides, a SERS substrate based on photonic semiconductor microarray was developed to form TiO<sub>2</sub> inverse opal substrate.<sup>58</sup> This array has a photonic band gap dependent sensitivity (EF = 2 × 10<sup>4</sup> and LOD of 10<sup>-5</sup> M for methylene blue, Table 1) which can be adjusted by matching laser wavelength with band gap. Hybrid nanoparticles or substrates were also developed combining TiO<sub>2</sub> and SiO<sub>2</sub>. For instance, TiO<sub>2</sub> was used to coat silica NPs by atomic layer deposition.<sup>59</sup> This shell structure NPs showed a high sensitivity (EF = 3.63 × 10<sup>4</sup>) for methylene blue. *Allesandri et al.* developed similar material by synthesizing SiO<sub>2</sub>/a-TiO<sub>2</sub> a core shell spheres called T-rex were used to enhance the signal of glutamyl-cysteinyl-glycine also called glutathione, a tripeptide involved in the redox homeostasis of cells.<sup>69</sup> They showed that a Glutathione solution infiltrated into core-shell colloidal crystals of SiO<sub>2</sub>/a-TiO<sub>2</sub> exhibited a higher signal-to-noise ratio than a solution of Glutathione mixed with gold nanoparticles.<sup>70</sup> Using similar particles, *Bontempi et al.* identified the SERS effect of T-rex as due to the Mie-type resonances. The authors used T-rex for measuring environmental CO<sub>2</sub><sup>71</sup> and for probing lysine mono-methylation in histone H3 tail peptides.<sup>72</sup>

**Cu<sub>2</sub>O, WO<sub>3-x</sub>, Fe<sub>3</sub>O<sub>4</sub>.** Through surface defects strategies, *Lin* and co-workers have developed a cube-like (few μm) superstructure of Cu<sub>2</sub>O with metal comparable SERS effect (EF = 8 × 10<sup>5</sup>, LOD = 10<sup>-9</sup> M for R6G, Table 1).<sup>60</sup> The copper vacancies favors the adsorption of positively charged molecules, and the defected surface of nanostructure facilitates interfacial charge transfer between substrate and molecules. By creating oxygen vacancies, the WO<sub>3-x</sub> is able to achieve a highly efficient SERS effect (EF = 3.4 × 10<sup>5</sup>, LOD = 10<sup>-7</sup> M for R6G, Table 1).<sup>61</sup> *Lee et al.* tested the ability of magnetite (Fe<sub>3</sub>O<sub>4</sub>) and maghemite (γ-Fe<sub>2</sub>O<sub>3</sub>) to enhance the signal of organic molecules such as oxalate (a metabolite) and cysteine (an amino-acid). While magnetite is a conductive semi-metal capable of electromagnetically enhanced Raman signal of both oxalate and cysteine, maghemite, which is non-conductive at room temperature, did not display any relevant signal enhancement.<sup>73</sup> These oxides nanostructures show promising SERS effect, however, their applications in biomedicine have not yet been addressed.

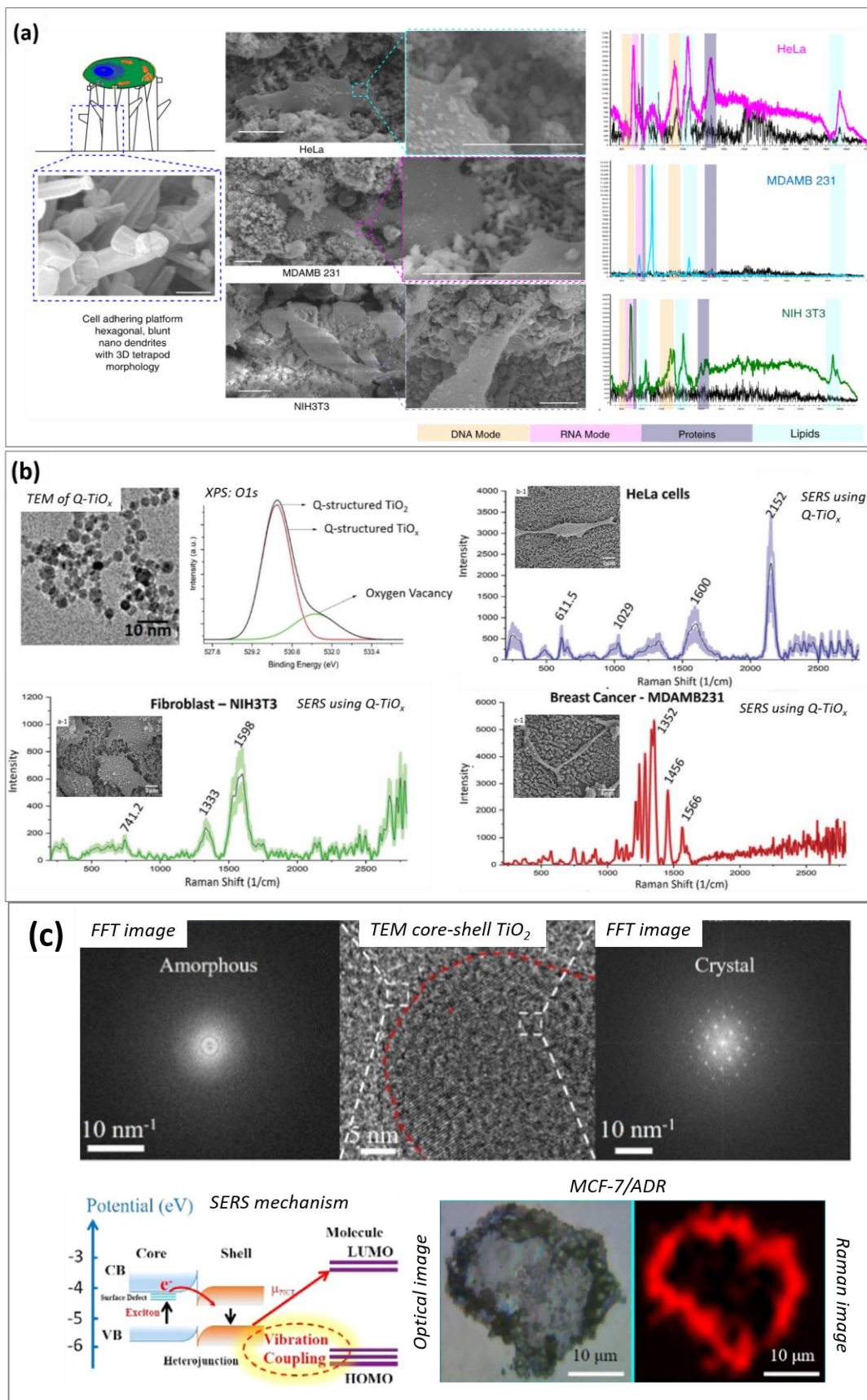


**Figure 4.** (a) Nano dendrites supported ZnO quantum probes for cell adhesion (SEM image scale = 10  $\mu\text{m}$ ) and the SERS (colored) / Raman (black) spectra of cells. Reproduced (Adapted) with permission from Ref. 54,

Copyright 2018, Springer Nature. (b) TEM image of Q-structured  $\text{TiO}_x$  (Q- $\text{TiO}_x$ ); comparison of O 1s spectra for Q-structured  $\text{TiO}_2$  and  $\text{TiO}_x$ ; the SERS spectra obtained in normal (inset: SEM of fibroblast interacted with Q- $\text{TiO}_x$ ) and cancerous (insets: SEM of HeLa and MDAMB231 interacted with Q- $\text{TiO}_x$ ) cells incubated with Q- $\text{TiO}_x$  for 12h. Reproduced (Adapted) with permission from Ref. 55, Copyright 2020, Royal Society of Chemistry. (c) TEM image of crystal-amorphous core-shell  $\text{TiO}_2$  NPs with fast Fourier transform (FFT) image of core and shell zone; Illustration of SERS mechanism; and optical / Raman imaging results of a cancer MCF-7/ADR cell incubated with functionalized core-shell  $\text{TiO}_2$  NPs for 1h. Reproduced (Adapted) with permission from Ref. 57, Copyright 2020, American Chemical Society.

### 3.3. Chalcogenides

Various studies undertaken in the last decade have revealed that semiconducting substrates, such as metal chalcogenides can expand the range of available SERS-active materials.<sup>74</sup> Indeed, compared to metals, these materials present several advantages such as their low cost, their stability, easy surface functionalization and tunable band gap. However, their main limitation arises from the relatively low enhancement factors that they can achieve. For this reason, the number of studies devoted to these SERS active substrates is still very limited. A description of the efforts that have been made these recent years in order to improve the SERS activity of metal chalcogenide substrates is presented below, emphasizing the key roles of various parameters such as particle size, shape, defect, heterostructure, chemical doping and stoichiometric ratio. This section will focus on the synthesis of (i) OD metal chalcogenide-based nanomaterials with different sizes and shapes and (ii) 2D nanostructures, from semiconducting to metallic phases.

**OD transition metal chalcogenides.** Although an enhancement of the Raman spectra of 4-mercaptopyridine has been reported on ZnS nanocrystals,<sup>75</sup> SERS-active OD chalcogenide nanomaterials are mainly based on copper sulfide (CuS). CuS is a typical p-type semiconductor with unique characteristics such as low cost and toxicity, high structural stability and absorption coefficient in sunlight. Interestingly, CuS nanostructures with different morphologies (microflowers, nanodendrites, hollow particles) and stoichiometry could be prepared in order to optimize enhancement factors and boost SERS efficiency. For example, hierarchical flower-like CuS microspheres with an average diameter of 1-4  $\mu\text{m}$  were synthesized using a simple hydrothermal approach.<sup>76</sup> The resulting particles exhibited either numerous and sparse petals or piled sheets, as observed on the SEM images Figure 5 (a-c). Using crystal violet (CV), malachite green (MG) and rhodamine 6G (R6G) as model analytes, enhancement factor of  $10^5$  were obtained with a detection

limit down to  $10^{-8}$  M for MG and  $10^{-7}$  M for CV and R6G (Table 1). This strong enhancement was shown to arise from both electromagnetic near-field effects and charge transfer between the reporter molecules and CuS. Interestingly, the morphology of the hierarchical CuS microflowers (number and spacing of petals) was observed to be a key parameter for Raman enhancement. Indeed, the flower-like CuS structures exhibiting the highest petal density yielded the strongest enhancement effect. This trend was supported by numerical simulations, which showed that the strongest field intensity was located between the petals. Multi-branched CuS nanodendrites could also be prepared by 1064 nm laser ablation of a bulk Cu target in thioacetamide solution.<sup>77</sup> The resulting nano-architectures exhibited elongated branches with an average length and diameter of about 20 nm and 6 nm, respectively. Owing to the presence of numerous nanotips, the CuS nanodendrites displayed high SERS activities for CV probes, comparable to that of noble-metal nanostructures, with a detection limit down to ca.  $10^{-10}$  M (Table 1). Moreover, CV molecules could be efficiently removed from the nanostructure surface after 60 cycles of SERS analysis, via moderate thermal treatment induced by 1064 nm laser irradiation, thus revealing an excellent reusability of the substrate. When picosecond or femtosecond pulses were used for the laser ablation of Cu targets in liquid media, periodic CuS nanostructures were obtained, allowing the trace level detection of explosive molecules.<sup>78</sup>

Another strategy was proposed to further improve the enhancement factors of CuS substrates, based on the elaboration of non-stoichiometric copper sulfide nanostructures.<sup>79</sup> Indeed, the abundant valence states of copper sulfide allows a fine tuning of its atomic ratio, leading to various electronic structures and related SERS activity. Copper sulfide nanostructures with different  $\text{Cu}_{7.2}\text{S}_4$  contents were synthesized using a hydrothermal method followed by mild heat treatment. The introduction of  $\text{Cu}_{7.2}\text{S}_4$  was shown to significantly improve the SERS performance of the substrate for the detection of R6G probes, and DFT calculations evidenced a SERS mechanism based on charge transfer resonance.

The toxicity issue and non-biodegradability of current SERS probes based on Au or Ag nanostructures was tackled by designing new photodegradable CuS SERS Probes. This constitutes a major challenge as the long-term persistence of nanomaterials within the body may induce chronic toxicity, thereby preventing translation to clinics. To meet this challenge, hollow CuS NPs were synthesized by reacting  $\text{Cu}_2\text{O}$  particles with  $\text{Na}_2\text{S}$  solution (Figure 5 d-e).<sup>80</sup> Raman reporters were

adsorbed on their surface and the NPs were then protected by poly(ethyleneglycol) (PEG) layers resulting in a hydrodynamic diameter of  $\sim 126$  nm. The hollow nature of the CuS NPs was shown to make them photodegradable upon NIR light irradiation, leading to the dissemination of small clusters, and can be easily cleared from the body, thus decreasing long-term toxicity. Moreover, these novel CuS SERS probes combined SERS efficiency and photothermal therapeutic activity, offering threefold attractive properties for Raman imaging, therapy and photodegradation.

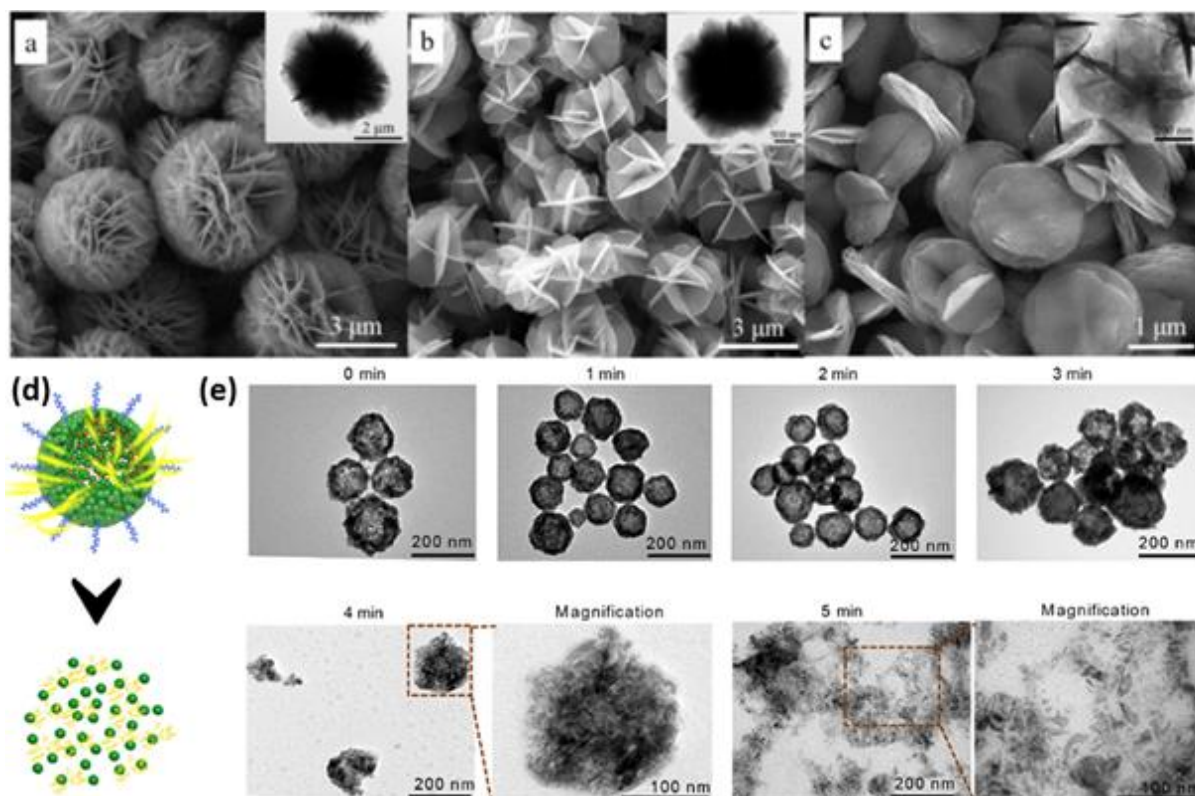
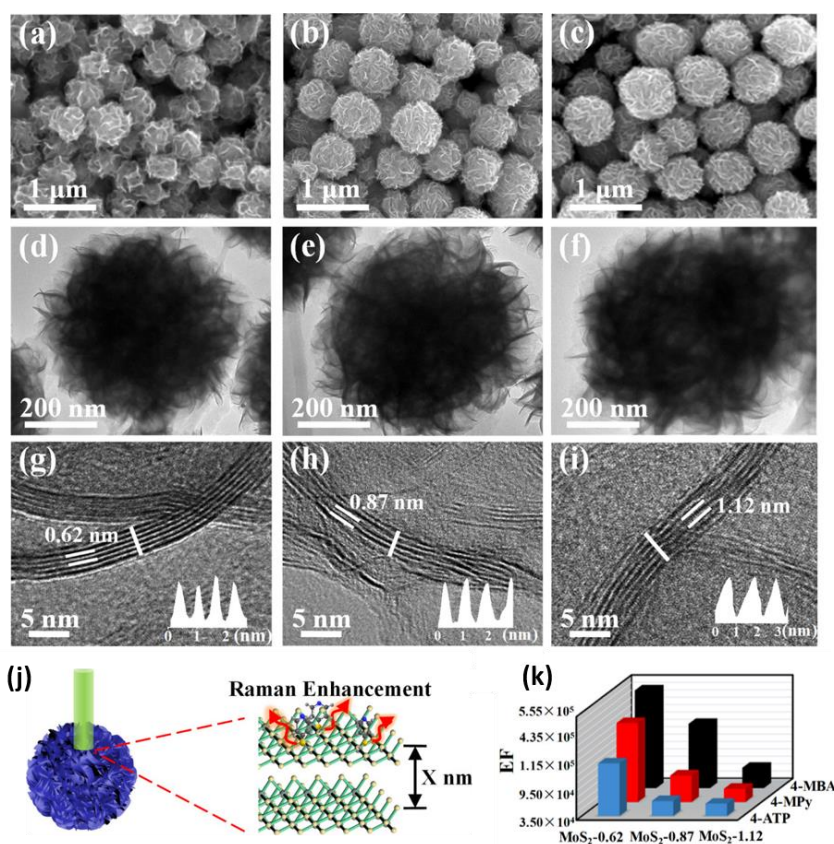


**Figure 5.** (a-c) SEM images of hierarchical flower-like CuS microspheres exhibiting (a) numerous petals, (b) sparse petals and (c) piled sheets. Insets shown the corresponding typical TEM images. Reproduced (Adapted) with permission from Ref. 76, Copyright 2021, Elsevier. (d) Representative scheme of the laser-induced photodegradation of hollow CuS SERS probes. (e) Typical TEM images of CuS hollow particles under continuous laser irradiation (980 nm, 800 mW) for 1–5 min. Reproduced (Adapted) with permission from Ref. 80, Copyright 2019, American Chemical Society.

**2D transition metal chalcogenides.** Recently, two-dimensional layered (2D) transition-metal dichalcogenides have attracted interest as a new class of SERS substrates due to their flat atomic surface allowing uniform chemisorption of probe molecules and favoring stable and repeatable signals, a key feature for standardized methodologies and practical applications. This class of

material can be divided into (i) semiconducting or (ii) metallic transition-metal dichalcogenides depending on the coordination and oxidation of the metal.<sup>81</sup>

**(i) Semiconducting transition-metal dichalcogenides:** among the semiconducting phases, molybdenum disulfide (MoS<sub>2</sub>),<sup>82, 83</sup> tungsten disulfide (WS<sub>2</sub>)<sup>19, 84</sup> and rhenium disulfide (ReS<sub>2</sub>)<sup>85, 86</sup> were shown to exhibit SERS activity via dipole–dipole coupling and weak charge transfer. In order to further improve their SERS efficacy, several approaches have been tested, based on either phase-transition engineering,<sup>87</sup> treatment via a plasma of MoS<sub>2</sub> nanoflakes,<sup>88</sup> tuning of the interlayer spacing<sup>89</sup> (Figure 6) or oxygen incorporation.<sup>90</sup>

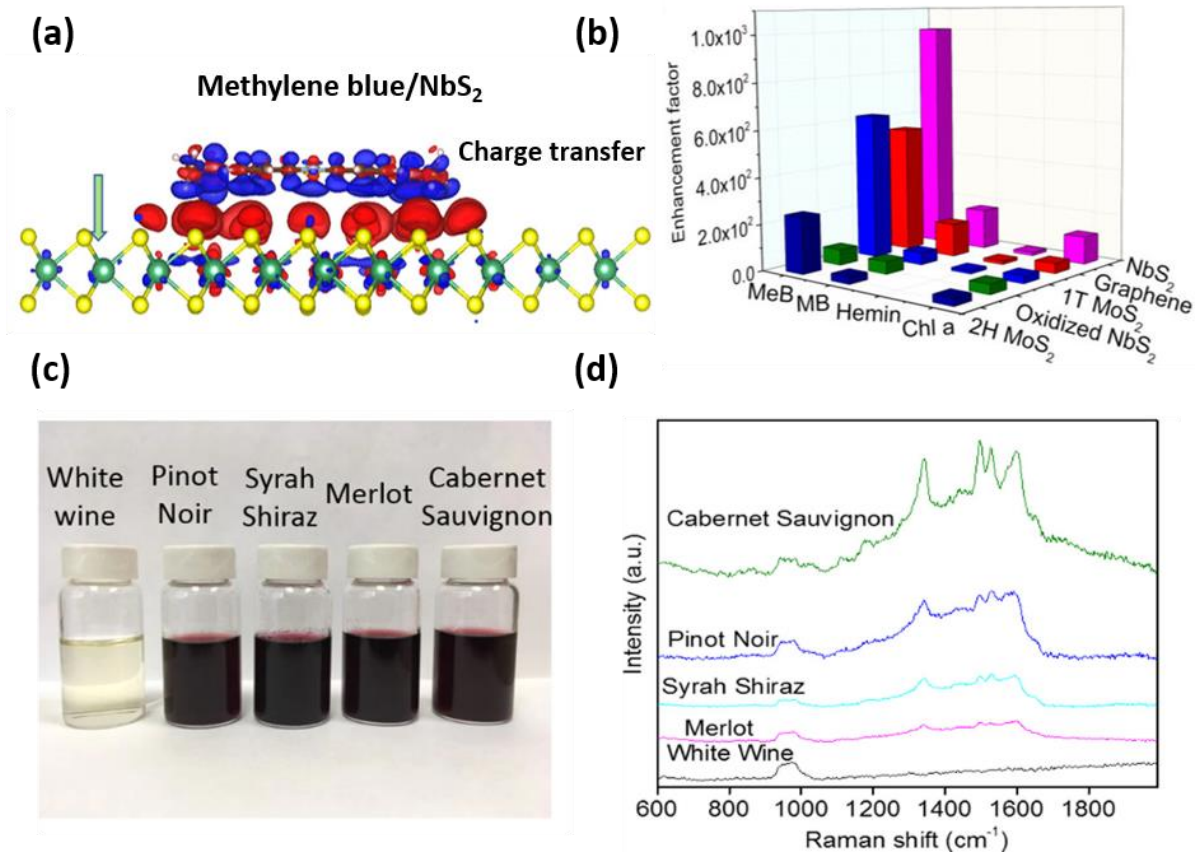


**(R2-7) Figure 6.** (a–c) Typical SEM images of MoS<sub>2</sub>-0.62 (a), MoS<sub>2</sub>-0.87 (b), and MoS<sub>2</sub>-1.12 (c); (d–f) corresponding TEM images and (g–i) HRTEM images. Insets in Fig. (g–i) represent the line profiles measured from the white lines in (g–i) for the MoS<sub>2</sub> lattice constants of 0.62, 0.87, and 1.12 nm. (j) Scheme of Raman enhancement on MoS<sub>2</sub> microspheres with different interlayered spacing. (k) EFs of MoS<sub>2</sub>-0.62, MoS<sub>2</sub>-0.87, and MoS<sub>2</sub>-1.12, probed with 4-MBA, 4-MPy, and 4-ATP. Reproduced (Adapted) with permission from Ref. 89, Copyright 2020, American Chemical Society.

The introduction of atomic vacancies in the lattice of WSe<sub>2</sub> was reported as another means to enhance the Raman scattering effect. Indeed, non-stoichiometric WSe<sub>2-x</sub> (x = 0-0.08) prepared by

bombarding stoichiometric WSe<sub>2</sub> with an ion beam, provided a 40-fold increase of the enhancement factor compared to pristine WSe<sub>2</sub>.<sup>91</sup> Interestingly, ternary nanocomposites made of ZnO, ZnS and MoS<sub>2</sub> were reported to provide higher SERS sensitivity and stability than their mono- or bi-component counterparts.<sup>92</sup> The porous structure of these ternary materials allows increasing the number of adsorption sites. In addition, they exhibit self-cleaning properties upon UV irradiation and can be reused without loss of activity for more than 5 detection cycles. However, despite these efforts and the significant progress achieved, the limits of detection in the previous reports are still inferior to those obtained with noble metal plasmonic materials. Therefore, the development of alternative approaches in order to improve the charge transfer efficiency on 2D transition-metal dichalcogenides still remains an important challenge.

**(ii) *Metallic transition-metal dichalcogenides:*** the use of metallic transition-metal dichalcogenides can meet this challenge as these materials possess abundant density of states near the Fermi level and high surface activity leading to efficient charge transfer with molecules adsorbed on their surface.<sup>93</sup> Niobium diselenide (NbSe<sub>2</sub>) is a typical 2D metallic transition-metal dichalcogenides, exhibiting a layer-dependent electronic structure. Large-area NbSe<sub>2</sub> flakes from monolayers to few-layers were prepared using an ambient pressure chemical vapor deposition route.<sup>94</sup> The six layer-substrates allowed the detection of extremely low concentrations of Rhodamine 6G (down to  $5 \times 10^{-16}$  M, cf. Table 1), around five times less than the value detected with only one layer, evidencing efficient charge transfer with the probe molecules. Similarly, the preparation of ultrathin niobium disulfide (NbS<sub>2</sub>) flakes (< 2.5 nm) with a large domain size (> 160  $\mu$ m), *via* alkali-assisted chemical vapor deposition,<sup>95</sup> yielded excellent SERS substrates, with a femtomolar detection limit for methylene blue and the capacity to distinguish different types of red wines (Figure 7).



**(R2-8) Figure 7.** (a) Scheme of charge-transfer mechanism between methylene blue and NbS<sub>2</sub>. (b) Enhancement factors for methylene blue, methyl blue, hemin, and chlorophyll a on NbS<sub>2</sub>, 1T MoS<sub>2</sub>, oxidized NbS<sub>2</sub>, graphene, and 2H MoS<sub>2</sub>. (c) Picture of five wines analyzed by SERS. (d) SERS spectra of Cabernet Sauvignon, Pinot noir, Syrah/Shiraz, Merlot and white wine on 3 nm thick NbS<sub>2</sub>. Reproduced (Adapted) with permission from Ref. 95, Copyright 2019, American Chemical Society.

### 3.4. Polymers, Telluride and Si

**Semi-conductive and conductive polymers.** Semi-conductive and conductive polymers display attractive properties such as controllable electrochemical characteristics and excellent mechanical processing.<sup>96, 97</sup> Since their discovery, they have quickly played an important role in the fields of flexible electronic devices, diodes and transistors, energy storage and biological electronic sensing.<sup>98</sup> In 2017, *Yilmaz et al.* synthesized semi-conductive and  $\pi$ -conjugated organic films composed of  $\alpha,\omega$ -diperfluorohexylquaterthiophene (DFH-4T, Figure 8a) by physical vapor deposition (PVD) method, and discovered their unexpected SERS activity for the first time, opening up a new way for the design of non-plasmonic substrates.<sup>99</sup> When methylene blue (MB) is used as a Raman probe molecule, as shown in Figure 8b, the EF of this DFH-4T film can be up to  $3.4 \pm 1.3 \times 10^3$  (Table 1), almost reaching the maximum value predicted by the chemical enhancement mechanism theory. Unlike other SERS

platforms with a contact angle  $<100^\circ$ , the hydrophobicity of DFH-4T film results in a contact angle of  $\sim 150^\circ$  for MB droplets, so that the MB molecules can be confined in an extremely small area to achieve the hydrophobicity-enhanced concentration effect. On the other hand, the significant  $\pi$ - $\pi$  stacking of the MB and substrate molecules promotes charge transfer between them and also contributes to the final chemical enhancement. What's more, the charge transfer resonance between analyte and the substrate vibronically couples with the nearby molecular transition, so the DFH-4T system can provide additional SERS enhancement.<sup>100</sup> These factors together lead to the amazing SERS activity of the DFH-4T film. Inspired by this research, *Zhang et al.* studied the SERS performance of poly(3,4-ethylenedioxythiophene):poly(styrenesulfonate) (PEDOT:PSS), a kind of conductive polymer with longer main chains and more regular  $\pi$ - $\pi$  stacking.<sup>18</sup> The EF of PEDOT:PSS film used for MB molecule detection can reach  $2.26 \times 10^3$  (Table 1). It is worth noting that because PEDOT:PSS can be regarded as a semi metallic material, lots of electrons can be excited and collectively oscillate under laser excitation, which leads to the surface plasmon resonance effect. The charge transfer and SPR effects work together to give the PEDOT:PSS film a high SERS enhancement factor.

**Telluride (semi)metals.** Due to their high surface activity and large available energy level distribution near the Fermi level, 1T' transition metal telluride semimetals are expected to be promising candidates for the design of noble-metal-free SERS substrates.<sup>101, 102</sup> *Li et al.* prepared large-scale 1T' transition metal telluride 2D layers (1T'-W(Mo)Te<sub>2</sub>) by chemical vapor deposition (CVD) method and realized ultralow concentration detection of Rhodamine 6G (R6G) molecules (Figure 8c and Table 1).<sup>103</sup> The detection limit of 1T'-W(Mo)Te<sub>2</sub> platform for R6G can reach 40 (400) fM, while the corresponding EF can rise up to  $1.8 \times 10^9$  ( $1.6 \times 10^8$ ), which is comparable to the values obtained with SERS substrates based on coinage metals. The high surface activities of 1T'-W(Mo)Te<sub>2</sub> layer, large dipoles and quasi-covalent bonds which can be formed between R6G molecules and the atomic layer, result in more effective electron transfer (Figure 8d), and thus greatly increase the Raman scattering cross-section of the analyte. In addition, the large density of states of 1T'-W(Mo)Te<sub>2</sub> near the Fermi levels further increases the probability of charge transition (Figure 8e). Meanwhile, the large charge transfer in the analyte-atomic layer complex leads to molecular fluorescence quenching, which is beneficial to improve the accuracy of the Raman signal.

**Metal-organic frameworks (MOFs)**, also called coordination polymers, are a novel kind of porous crystalline material formed by the combination of metal nodes and organic ligands.<sup>104</sup> Thanks to their unique porous morphology, MOFs have been widely used in the fields of gas adsorption, storage, separation and catalysis.<sup>105, 106</sup> Interestingly, the MIL-100(Fe) platform designed by *Fu et al.*<sup>107</sup> (Figure 8f) can be used as plasmon-free SERS-active substrate for the detection of volatile organic compounds (VOCs). DFT calculations proved that the enhanced charge transfer leads to the high SERS activity of this MOFs system (Figure 8g). The detection limit of toluene can reach 2.5 ppm (Table 1), which is much higher than the detection limit of traditional gas sensors. Moreover, MIL-100(Fe) platform also shows high sensitivity and selectivity in the monitoring and identification of lung cancer gas indicators, offering great potential in the early diagnosis of lung cancer.

**Silicon.** Generally, Si is used as a substrate for the synthesis of two-dimensional SERS materials and does not provide SERS enhancement. However, the 3D near-quantum-scale Si nanomesh prepared by Jeffrey et al. via ionizing single-crystal defect-free Si wafers shows excellent plasmon-free SERS activity.<sup>108</sup> By adjusting the ionization energy and ion-ion interaction, as shown in Figure 8h, the near quantum-scale defects in the 3D Si structure can be effectively controlled and engineered to change its SERS activity and activate the CT enhancement of Si nanomesh. In this work, both the enriched crystallographic defects and nanomesh morphology should be responsible for the SERS effect. As shown in Figure 8i, the created structure defects (near quantum scale defects and grain boundary disorder) could increase Raman photon scattering. Meanwhile the mesh structure would “trap” biomolecules on the surface. This Si only nanomesh system could monitor various disease biomarkers (L-glutathione, tryptophan, cysteine and methionine) at very low concentrations (from  $10^{-9}$  M to  $10^{-6}$  M), providing new opportunities for the application of Si materials as non-plasmonic SERS materials.

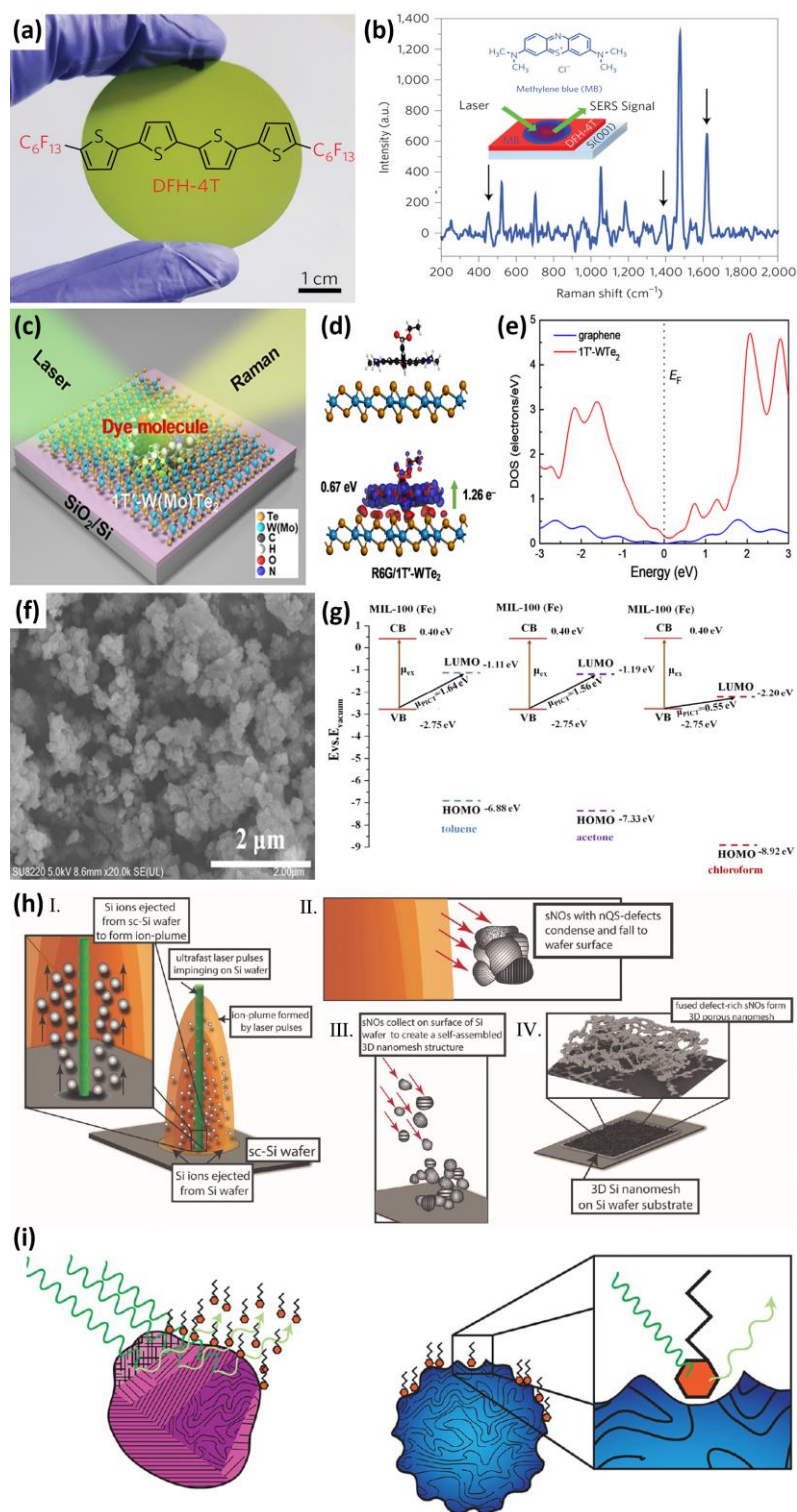


**Figure 8.** (a) Photograph of the DFH-4T film (the inset is the corresponding chemical structure); (b) SERS spectra of MB molecule on DFH-4T films. Reproduced (Adapted) with permission from Ref. 99, Copyright, 2017, Springer Nature. (c) Schematic illustration of the 1T' transition metal telluride 2D layer platform (1T'-W(Mo)Te<sub>2</sub>) for SERS detection; (d) Side view of the electron density isosurface of chemically adsorbed R6G on 1T'-WTe<sub>2</sub>; (e) The density of states of the 1T'-WTe<sub>2</sub> layer near the Fermi levels. Reproduced (Adapted) with permission from Ref. 103, Copyright, 2018, American Chemical Society. (f) SEM image of MIL-100(Fe) platform; (g) Energy-level illustrations of the target VOCs analytes (toluene, acetone and chloroform) relative to MIL-100(Fe), with respect to the vacuum level. Reproduced (Adapted) with permission from Ref. 107, Copyright, 2020, Wiley. (h) Schematic of the 3D Si nanomesh fabrication process. (i) Schematic of the SERS detection mechanism on the 3D Si nanomesh.

Schematic diagram of synthesis process of the 3D Si nanomesh growth. (i) Illustration of the non-plasmonic SERS enhancement of 3D Si nanomesh, which derived from the increased Raman photon scattering caused by the nQS grain boundary disorder and the trapped molecules in the nQS voids on the surface of Si subnano-orbs. Reproduced (Adapted) with permission from Ref. 108, Copyright, 2017, American Chemical Society.

**Table 1.** Substrates for non-plasmonic detection with excitation laser wavelengths  $\lambda_{ex}$ , reference molecular probe, limit of detection, maximum enhancement factors (EF).

Substrate (laser $\lambda_{ex}$ )	Probe	LOD (M)	Enhancement factor (EF)	Ref
<b>Carbons</b>				
<b>0D graphene quantum dots (GQDs)</b>				
GQDs-Mn <sub>3</sub> O <sub>4</sub> ( $\lambda_{ex}$ = 514 nm)	Rhodamine B	-	$2.06 \times 10^4$	43
N-GQDs ( $\lambda_{ex}$ = 488 nm)	Rhodamine B	$10^{-10}$	$3.2 \times 10^3$	44
<b>1D carbon nanotubes (CNTs)</b>				
R/L-CNTs/TiO <sub>2</sub> ( $\lambda_{ex}$ = 532 nm)	Methylene blue	$5 \times 10^{-5}$	-	24
<b>2D Graphene</b>				
EG-TiO <sub>2</sub> ( $\lambda_{ex}$ = 633 nm)	CuPc	$6 \times 10^{-5}$ ( $2.07 \times 10^{-16}$ IU)	48.2	49
Graphene flask ( $\lambda_{ex}$ = 633 nm)	Hemoglobin	-	4.5	50
GMFs/W-MoS <sub>2</sub> ( $\lambda_{ex}$ = 632.8 nm)	Rhodamine B	$5 \times 10^{-11}$	$2.96 \times 10^7$	51
<b>3D interconnected nanocarbon web (INW)</b>				
INW ( $\lambda_{ex}$ = 785 nm)	Crystal violet	-	$3.66 \times 10^4$	9
<b>Oxides</b>				
<b>Zinc oxide</b>				
Amorphous ZnO nanocages ( $\lambda_{ex}$ = 633 nm)	4-MBA, 4-MPY, and 4-ATP	$10^{-4}$	$6.62 \times 10^5$	53

ZnO quantum probe ( $\lambda_{ex} = 785$ nm)	crystal violet and rhodamine 6G, 4-Adenosine triphosphate, 4-Mercaptobenzoic	$10^{-9}$	$1.4-6.9 \times 10^6$	54
<b><i>Titanium oxide</i></b>				
Quantum-structured TiO <sub>x</sub> ( $\lambda_{ex} = 785$ nm)	Crystal violet	$10^{-9}$	$3.4 \times 10^7$	55
Crystal-amorphous core-shell TiO <sub>2</sub> ( $\lambda_{ex} = 532$ nm)	4-nitrobenzenthioi	$5 \times 10^{-4}$	$4.3 \times 10^5$	57
silica NPs coated with TiO <sub>2</sub> ( $\lambda_{ex} = 783$ nm)	Methylene Blue and Dopamine	$10^{-2}$	$3.63 \times 10^4$	59
Atomic-defect quantum probe of TiO <sub>2</sub> ( $\lambda_{ex} = 785$ nm)	Crystal violet	$10^{-9}$	$10^{10}$	56
TiO <sub>2</sub> inverse opal substrate ( $\lambda_{ex} = 532$ nm)	Methylene blue	$10^{-5}$	$2.0 \times 10^4$	58
<b><i>Copper and tungsten oxide</i></b>				
Cu <sub>2</sub> O cubic super structure ( $\lambda_{ex} = 647$ nm)	Rhodamine 6G Crystal violet Methyl Blue Methyl Orange	$10^{-7}$	$1.5 \times 10^4 - 8 \times 10^5$	60
WO <sub>3-x</sub> ( $\lambda_{ex} = 532.8$ nm)	Rhodamine 6G	$10^{-7}$	$3.4 \times 10^5$	61
<b><i>Transition metal chalcogenides</i></b>				
<b><i>0D transition metal chalcogenides</i></b>				
<b>ZnS</b> nanocrystals ( $\lambda_{ex} = 514.5$ nm)	4-mercaptopyridine	$10^{-6}$	$10^3$	75
<b>CuS</b> microflowers ( $\lambda_{ex} = 532$ or 633 nm)	Crystal violet, malachite green, rhodamine 6 G	$10^{-8}$ for MG $10^{-7}$ for R6G and CV	$10^5$	76
Multi-branched <b>CuS</b> nanodendrites	Crystal violet	$10^{-10}$	-	77
Hollow <b>CuS</b> NPs ( $\lambda_{ex} = 785$ nm)	3,3'-diethylthiatricbo cyanine iodide	$10^{-12}$	$3.9 \times 10^2 - 4.6 \times 10^4$	80
<b><i>2D transition metal chalcogenides</i></b>				

2D MoS <sub>2</sub> monolayer ( $\lambda_{\text{ex}} = 488$ nm)	4-Mercaptopyridine	-	$\sim 10^5$	83
Oxygen incorporated MoS <sub>2</sub> ( $\lambda_{\text{ex}} = 532.8$ nm)	Rhodamine 6G	Below $10^{-7}$	$\sim 10^5$	90
MoS <sub>2</sub> microspheres with different interlayered spacings ( $\lambda_{\text{ex}} = 785$ nm)	4-mercaptopyridine (4-MPy), 4-mercaptobenzoic acid (4-MBA), and 4-aminothiophenol (4-ATP)	-	$5.31 \times 10^5$	89
Ultrathin 2D NbS <sub>2</sub>	Methylene blue	$10^{-14}$	$\sim 10^3$	95
Large-area NbSe <sub>2</sub> flakes from monolayer to few-layer	Rhodamine 6G	$5 \times 10^{-16}$	-	94
Ternary ZnO/ZnS/MoS <sub>2</sub> nanoflake composite	Rhodamine 6G	$10^{-9}$	$1.4 \times 10^8$	92
<b>Polymers, telluride and Si</b>				
DFH-4T films ( $\lambda_{\text{ex}} = 785$ nm)	Methylene blue	-	$3.4 \pm 1.3 \times 10^3$	99
PEDOT:PSS film ( $\lambda_{\text{ex}} = 514$ nm)	Methylene blue	-	$2.26 \times 10^3$	18
2D 1T'-W(Mo)Te <sub>2</sub> layers ( $\lambda_{\text{ex}} = 532$ nm)	Rhodamine 6G	40 (400) fM	$1.8 \times 10^9$	103
MIL-100(Fe) MOF array ( $\lambda_{\text{ex}} = 785$ nm)	Toluene, acetone and chloroform	2.5, 20 and 92.7 ppm	$10^5$	107
3D nQS Si nanomesh ( $\lambda_{\text{ex}} = 532$ and 785 nm)	L-glutathione, tryptophan, cysteine and methionine	$10^{-9}$ M	$\sim 10^2$	108

#### 4. Non plasmonic SERS for biomedical sciences: *Surface functionalization or not?*

SERS is a very sensitive analytical technology which makes it possible to acquire molecular insights in complex biological samples. Moreover, the rich vibrational information of SERS spectra is ideal for multiplex biosensing,<sup>109</sup> offering unprecedented opportunities for various biomedical applications. To

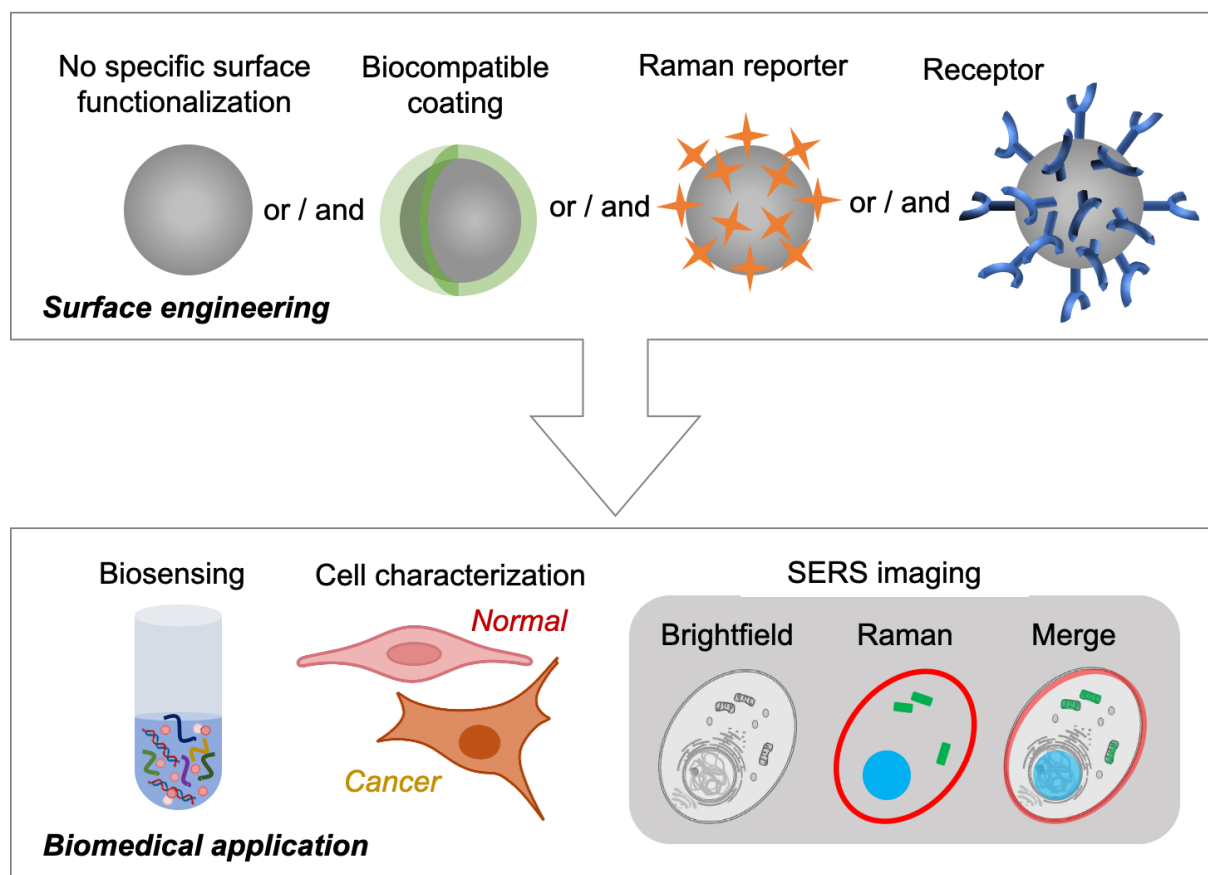
achieve efficient and safe SERS-based bioapplications, it is very important to control the surface of substrates. Surface functionalization can be used to immobilize biocompatible coating, Raman tags or/and targeting (receptor) molecules, as shown in Fig. 9 and Table 2. The detection of molecules using SERS can be based on either (i) direct detection, also called label-free analysis, using NPs without specific labeling or (ii) indirect detection.

**(i) Direct detection.** In the case of direct detection, SERS provides information on the NP environment by sensing the surrounding medium. For example, SERS signals from DNA, RNA, protein and lipid could be obtained in cells after uptake of ZnO nanoprobables.<sup>54</sup> This direct SERS method avoids additional surface modification steps. However, as the environment of NPs is very complex in biological media, with the presence of several biomarkers at the same time, it can be complicated to obtain robust data with label-free SERS.<sup>54</sup> Recently, machine learning has been reported to analyze spontaneous Raman (non-SERS) spectra for the differentiation of cancer and normal tissue.<sup>110</sup> Such a technique has also been used to analyze wine flavor based on plasmonic SERS signals from an “artificial taster”.<sup>111</sup> Therefore, machine learning would be a promising approach to promote label-free SERS substrates in biomedical applications. It is worth noting that surface engineering is not necessary for direct detection on chips, biopsy or ex vivo analysis,<sup>50, 112</sup> whereas it is essential for *in vitro* or *in vivo* analysis because NPs will be uptaken and will participate in biological processes. For most SERS NPs, biosafety is the premier and the main concern. Physicochemical properties, like particle size, charge, crystallinity, shape, concentration and agglomeration state, may have a strong biological impact.<sup>113</sup> Thus, synthesis of colloidal NPs with controlled size, morphology and surface is highly recommended. The main approach is surface functionalization with biocompatible coating, which could be *in situ* formed during synthesis or introduced later by post-functionalization and ligand-exchange. For example, bare ZnO NPs exhibit poor stability in water, resulting in poor cell uptaking. To solve this problem, *Zhao et al* have synthesized ester and silane coated ZnO which show good biocompatibility in hemolysis assay.<sup>68</sup> To prolong NPs retention time and prevent opsonization,<sup>114</sup> hollow CuS NPs were post-functionalized with polyethylene glycol coating and used as SERS imaging agents for *in vivo* cancer theranostics.<sup>80</sup>

**(ii) Indirect detection.** In the case of indirect detection, the preparation of the label SERS requires a supplementary surface functionalization process to immobilize Raman reporters.<sup>115</sup> This configuration gives the opportunity to follow and track the signals from the Raman tags. The most commonly used labeling molecules are based on small dyes and thiols coupling agents. For example, Raman reporters based on thiols (3,3'-diethylthiatricarbocyanine iodide, 3,3'-diethylthiadcarbocyanine iodide and 3,3'-diethylthiacarbocyanine iodide) have been adsorbed on CuS substrates for plasmon-free SERS imaging of cancer tissue.<sup>80</sup> However, these reporters suffer from 2 main shortcomings: (i) their Raman signals are located within the biological windows which make their tracking difficult in a biological environment and (ii) they undergo easy desorption from the substrate surface with a risk of signal loss with time. To overcome the first drawback, Raman reporters bearing cyano and alkyne groups have attracted lots of interest because their Raman peak (at 2000-2300  $\text{cm}^{-1}$ ) is in the cell silent window (1800-2600  $\text{cm}^{-1}$ ).<sup>116, 117</sup> For example, an alkyne-containing ligand has been synthesized and attached to Li-MoS<sub>2</sub> NPs for live WrDi cells Raman imaging.<sup>118</sup> Regarding the second drawback, it was shown that aryl diazonium salts could serve as an alternative approach to thiol analogues to graft reporters through stable surface-carbon bonds.<sup>119</sup> Raman reporters derived from aryl diazonium salts have been reported for SERS cell imaging using Au NP-based tags.<sup>120</sup> Interestingly, unlike thiols (which can be only used for metals and sulfites), diazonium salts can be used to graft a wide range of substrates, such as metals, carbons, oxides, polymers, phosphorus black, virus, amino acids, proteins, etc.<sup>121, 122</sup> Thanks to their promising features, these functionalized nanostructures have been used for various biomedical applications, including biosensing, bioimaging, drug delivery, antibacterials treatment, etc.<sup>121</sup>

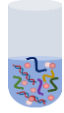
Surface functionalization of SERS substrates by receptors or targeting molecules would be particularly well suited for the specific detection of biomarkers. For example, amino-modified telomerase primers could be immobilized on TiO<sub>2</sub> surface and extended by telomerase to form telomere repeats (TTAGGG)<sub>n</sub>, which can monitor telomerase activity in presence of a Raman tag of CuPC.<sup>49</sup> One can also immobilize a receptor with specific recognition on SERS substrate, achieving recognition - separation - probing biosamples. *Bontempi et al* have functionalized core-shell SiO<sub>2</sub>-TiO<sub>2</sub> by supramolecular tetra-phosphonate cavitand as receptor to probe lysine mono-methylation in histone H3 tail peptides.<sup>72</sup> NPs can be also functionalized by targeting molecules to quickly distinguish

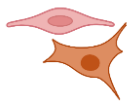
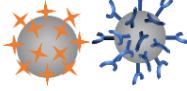
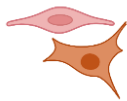
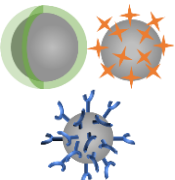
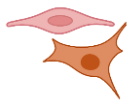
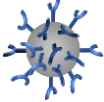
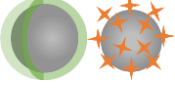
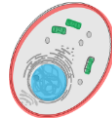
the target. For instance, an antibody (anti-P-glycoprotein) can be clicked to the polymer coating of TiO<sub>2</sub> NPs to target P-glycoprotein of drug-resistant breast cancer cells, favoring efficient delivery of SERS imaging agent.<sup>57</sup>

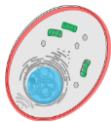


**Figure 9.** Surface engineering of SERS substrates, from the absence of surface modification to functionalization with biocompatible coating, Raman tag (reporter) or bio-receptor for biosensing, cell characterization and SERS imaging.

**Table 2.** Nanomaterials for non-plasmonic SERS detection and biomedical applications (see icon in Fig. 9).

Nanomaterial	Surface functionalization	Application		Ref.
GQDs-Mn <sub>3</sub> O <sub>4</sub> nanocomposite		Identification of cancer cells from normal cells		43
Monolayer graphene flakes		Sensing of hemoglobin and albumin		50

interconnected nanocarbon web (INW)		In vitro detection and differentiation of HeLa cells and fibroblasts		9
Graphene-TiO <sub>2</sub> nanocomposites		Real-time monitoring of telomerase activity in stem cells		49
SiO <sub>2</sub> /TiO <sub>2</sub> core-shell beads		Monitor the redox cycle of glutathione at physiological concentration as homeostasis model		70
Nano denstrite supported ZnO quantum probe		Identification of cancer cells from normal cells		54
Crystal-Amorphous Core-Shell TiO <sub>2</sub>		Cancer cell imaging		57
Q-structured TiO <sub>x</sub> (Q-TiO <sub>x</sub> )		Identification of cancer cells from normal cells		55
SiO <sub>2</sub> /TiO <sub>2</sub> core-shell beads		Recognition, separation and probing of lysine mono-methylated histone H3 tail peptides		72
Hollow CuS NPs		Cancer tissue imaging		80

lithium-exfoliated MoS <sub>2</sub>		Live cell imaging		118
3D near quantum scaled silicon		Detection of tripeptide biomarker (L-glutathione)		108

**What for?** Non-plasmonic nanostructures have been used for three types of biomedical applications (Figure 9 and Table 2): (i) the detection of biomarkers, (ii) the characterization of cell types such as the identification of cancer cells and (iii) the design of contrast agents for SERS imaging. Regarding biomarker detection, they have been used for the sensing of two main blood proteins, namely, hemoglobin and albumin on graphene substrates;<sup>50</sup> for real-time monitoring of telomerase activity in stem cells (using Graphene-TiO<sub>2</sub> nanocomposites);<sup>49</sup> for monitoring homeostasis mode by sensing the redox cycle of glutathione;<sup>70</sup> for detection of biomarker (L-glutathione) on quantum scaled Si or the detection of post-translational modification of Histone H3 (on core-shell SiO<sub>2</sub>-TiO<sub>2</sub>).<sup>72</sup> To characterize cell type, *Haldavnekar et al* described an engineered 3D assemblies of ZnO-based quantum probes on a nano-dendrite platform where the cells are able to attach and proliferate. The ZnO quantum dots were efficiently internalized by the cells. After fixation and drying of the cells, the Raman spectra obtained allowed the discrimination between cancer cells and non-cancer cells.<sup>54</sup> Another example was reported by *Lan et al.* where cancer and non-cancer cell lines were cultured on 3D assemblies of GCDs-Mn<sub>3</sub>O<sub>4</sub> nanocomposites. The spectra obtained from cells cultivated on such substrates were sufficiently enhanced for quantification and to discriminate between the two kinds of cells, based on a lipid/protein-DNA/RNA signal ratio.<sup>43</sup> Another substrate consisting in quantum-structured TiO<sub>2</sub> nanostructures were used to discriminate breast cancer cells and fibroblasts. This discrimination was based on the lipid/protein ratio together with a specific EGFR peaks.<sup>55</sup> Similarly, interconnected nanocarbon web could be applied for *in vitro* detection and differentiation of HeLa cells and fibroblasts from distinctive SERS band profile of lipids, proteins and DNA/RNA.<sup>9</sup> Non-plasmonic NPs could also serve for SERS imaging. For example, Alizarin Red modified TiO<sub>2</sub> NPs were used for cancer cell imaging;<sup>57</sup> alkyne conjugated MoS<sub>2</sub> for live cell imaging; cyanine-labeled CuS for cancer tissue imaging.<sup>80</sup> Regarding biosensing applications, the sensing results were obtained with pure solutions

of molecules. However, one challenge of this type of detection test is to be able to detect the target analytes from complex fresh samples, such as blood, or cell extracts. For cell characterization, the published results are all obtained on label-free SERS substrates, so the spectra might be very complex to analyse. The combination of artificial intelligence would be a promising way to interpret the complicated data. In SERS imaging, non-plasmonic NPs have shown great potential, but efforts should be devoted to developing Raman tag with specific, stable signal and good compatibility.

## Conclusion

This review presents a number of examples of nanostructures with non-plasmonic SERS effect for biomedical applications. The mechanisms leading to the improvement of Raman signals are first summarized, from the resonance effect to the electromagnetic (EM) or chemical enhancement (CM), fluorescence quenching and laser-driven birefringence. A description of the large range of nanomaterials (carbons, oxides, chalcogenides, polymers, semimetals, silicon, etc.) that can be used for non-plasmonic SERS detection is then provided. The main interests of these materials, compared with their plasmonic counterparts (e.g. noble Au and Ag NPs), are non-photothermal interference and low-cost. However, their EF value ( $< 10^3$ ) is usually lower than that of plasmonic SERS nanostructures ( $10^{10}$ - $10^{11}$ ). The main strategy to increase EF is to tailor the surface composition (ex.  $\text{Cu}_{7.2}\text{S}_4$  versus  $\text{Cu}_2\text{S}$ ), defect (ex. oxygen vacancies in  $\text{TiO}_x$  and  $\text{WO}_{3-x}$ ), morphology (ex. porous 3D carbon network, mesh Si and MOF) and energy level (ex. shifted Fermi level of graphene- $\text{TiO}_2$  composite, heterojunction of crystal-amorphous core-shell  $\text{TiO}_2$  NPs) of the substrate. The combination of CM with fluorescence quenching (ex. GQDs- $\text{Mn}_3\text{O}_4$  nanocomposite) and birefringence (ex. chiral CNTs/ $\text{TiO}_2$ ) are also efficient approaches to achieve sensitive SERS. Through these strategies, the EF of non-plasmonic SERS nanostructures can achieve up to  $10^{10}$ , comparable to the values obtained with plasmonic SERS substrates, opening promising prospects for bioimaging, sensing and biomolecule tracking.

However, the examples of biomedical applications of non-plasmonic SERS materials are limited to proofs of concept. Several challenges still need to be addressed to boost practical and real-world applications for both direct and indirect plasmon-free SERS detection. A key issue concerns biosafety with the necessity to select the appropriate materials in order to develop non-toxic nanostructures for both *in vitro* and *in vivo* applications. Biocompatibility can be further improved via NPs surface

functionalization with protecting coatings such as organosilanes or polyethylene glycol. Besides, surface functionalization can also impart higher colloidal stability to the SERS nanoparticles. Regarding direct detection, the complexity of the Raman signals arising from the non-specific adsorption of biomolecules on the SERS substrate is a crucial issue. Although cell characterizations (normal/cancer) have been successfully performed using non-plasmonic SERS, the analysis of large amounts of data from tissue should be associated in the future with artificial intelligence (ex. big data analysis and machine learning). In the domain of indirect detection, the main bottle-necks are generally the low availability of Raman tags exhibiting signals in the biological-silent window (1800-2600  $\text{cm}^{-1}$ ) and suitable coupling agents for the attachment of bioreceptors. The most common used Raman tags, for example small dye molecules of MB and rhodamines, exhibit Raman peaks in the range of 500-1800  $\text{cm}^{-1}$ , and are thus hard to track in biological environment. In contrast, tags bearing  $-\text{CN}$  or  $-\text{CCH}$  groups (Raman shift at 2000-2300  $\text{cm}^{-1}$ ) are good candidates for SERS bioimaging. The conventional coupling agents to graft Raman reporters or receptors on the SERS substrates are thiols molecules, resulting in the formation of surface-S bonding. However, the use of thiols is mainly limited to metals and chalcogenides surfaces but it is inefficient for the functionalization of most non-plasmonic SERS substrates. Therefore, great efforts remain to be done to develop controllable and efficient surface functionalization strategies for the immobilization of Raman reporters or/and bioreceptors on non-plasmonic SERS substrates in order to achieve accurate, reliable, sensitive and specific bio-detection.

### Acknowledgments

This work is supported in part by the scholarship from China Scholarship Council (CSC) under the Grant CSC N° 201909370060.

### References

1. Antonio KA, Schultz ZD. Advances in biomedical Raman microscopy. *Anal Chem* 2014, 86:30-46.
2. Ellis DI, Goodacre R. Metabolic fingerprinting in disease diagnosis: biomedical applications of infrared and Raman spectroscopy. *Analyst* 2006, 131:875-85.
3. Baumberg JJ, Kelf TA, Sugawara Y, Cintra S, Abdelsalam ME, Bartlett PN, Russell AE. Angle-resolved surface-enhanced Raman scattering on metallic nanostructured plasmonic crystals. *Nano Lett* 2005, 5:2262-7.

4. Tripp RA, Dluhy RA, Zhao Y. Novel nanostructures for SERS biosensing. *Nano Today* 2008, 3:31-7.
5. Ngo HT, Wang H-N, Fales AM, Vo-Dinh T. Plasmonic SERS biosensing nanochips for DNA detection. *Anal Bioanal Chem* 2016, 408:1773-81.
6. Blackie EJ, Le Ru EC, Etchegoin PG. Single-molecule surface-enhanced Raman spectroscopy of nonresonant molecules. *J Am Chem Soc* 2009, 131:14466-72.
7. Naahidi S, Jafari M, Edalat F, Raymond K, Khademhosseini A, Chen P. Biocompatibility of engineered nanoparticles for drug delivery. *J Control Release* 2013, 166:182-94.
8. Campion A, Ivanecy III J, Child C, Foster M. On the mechanism of chemical enhancement in surface-enhanced Raman scattering. *J Am Chem Soc* 1995, 117:11807-8.
9. Chowdhury AKMRH, Tan B, Venkatakrisnan K. SERS-active 3D interconnected nanocarbon web toward nonplasmonic in vitro sensing of HeLa cells and fibroblasts. *ACS Appl Mater Interfaces* 2018, 10:35715-33.
10. Moskovits M. Persistent misconceptions regarding SERS. *Phys Chem Chem Phys* 2013, 15:5301-11.
11. Haidar I, Lévi G, Mouton L, Aubard J, Grand J, Lau-Truong S, Neuville DR, Félidj N, Boubekeur-Lecaque L. Highly stable silica-coated gold nanorods dimers for solution-based SERS. *Phys Chem Chem Phys* 2016, 18:32272-80.
12. Fleischmann M, Hendra PJ, McQuillan AJ. Raman spectra of pyridine adsorbed at a silver electrode. *Chem Phys Lett* 1974, 26:163-6.
13. Hao E, Schatz GC. Electromagnetic fields around silver nanoparticles and dimers. *J Chem Phys* 2003, 120:357-66.
14. Kelly KL, Coronado E, Zhao LL, Schatz GC. The optical properties of metal nanoparticles: the influence of size, shape, and dielectric environment. *J Phys Chem B* 2003, 107:668-77.
15. Félidj N, Aubard J, Lévi G, Krenn JR, Hohenau A, Schider G, Leitner A, Aussenegg FR. Optimized surface-enhanced Raman scattering on gold nanoparticle arrays. *Appl Phys Lett* 2003, 82:3095-7.
16. Ragheb I, Braïk M, Lau-Truong S, Belkhir A, Rumyantseva A, Kostcheev S, Adam P-M, Chevillot-Biraud A, Lévi G, Aubard J, Boubekeur-Lecaque L, Félidj N. Surface enhanced Raman scattering on regular arrays of gold nanostructures: impact of long-range interactions and the surrounding medium. *Nanomaterials* 2020, 10:2201-14.
17. Kerker M, Wang DS, Chew H. Surface enhanced Raman scattering (SERS) by molecules adsorbed at spherical particles. *Appl Opt* 1980, 19:3373-88.
18. Zhang X-Y, Yang S, Yang L, Zhang D, Sun Y, Pang Z, Yang J, Chen L. Carrier dynamic monitoring of a  $\pi$ -conjugated polymer: a surface-enhanced Raman scattering method. *Chem Commun* 2020, 56:2779-82.
19. Kim J, Jang Y, Kim N-J, Kim H, Yi G-C, Shin Y, Kim MH, Yoon S. Study of chemical enhancement mechanism in non-plasmonic surface enhanced Raman spectroscopy (SERS). *Front Chem* 2019, 7:582-9.

20. Ringler M, Schwemer A, Wunderlich M, Nichtl A, Kürzinger K, Klar TA, Feldmann J. Shaping emission spectra of fluorescent molecules with single plasmonic nanoresonators. *Phys Rev Lett* 2008, 100:203002.
21. Pons T, Medintz IL, Sapsford KE, Higashiya S, Grimes AF, English DS, Mattoussi H. On the quenching of semiconductor quantum dot photoluminescence by proximal gold nanoparticles. *Nano Lett* 2007, 7:3157-64.
22. Ru ECL, Grand J, Félidj N, Aubard J, Lévi G, Hohenau A, Krenn JR, Blackie E, Etchegoin PG. Spectral profile modifications in metal-enhanced fluorescence. *Metal-Enhanced Fluorescence* 2010. p. 25-65.
23. Sil S, Kuhar N, Acharya S, Umapathy S. Is chemically synthesized graphene 'really' a unique substrate for SERS and fluorescence quenching? *Sci Rep* 2013, 3:3336.
24. Qiu B, Xing M, Yi Q, Zhang J. Chiral carbonaceous nanotubes modified with titania nanocrystals: plasmon-free and recyclable SERS sensitivity. *Angew Chem Int Ed* 2015, 54:10643-7.
25. Jen Y-J, Liu W-C, Cong M-Y, Chan T-L. Bideposited silver nanocolloid arrays with strong plasmon-induced birefringence for SERS application. *Sci Rep* 2020, 10:20143.
26. Naik GV, Shalaev VM, Boltasseva A. Alternative plasmonic materials: beyond gold and silver. *Adv Mater* 2013, 25:3264-94.
27. Baffou G, Quidant R. Thermo-plasmonics: using metallic nanostructures as nano-sources of heat. *Laser Photonics Rev* 2013, 7:171-87.
28. Caldarola M, Albella P, Cortés E, Rahmani M, Roschuk T, Grinblat G, Oulton RF, Bragas AV, Maier SA. Non-plasmonic nanoantennas for surface enhanced spectroscopies with ultra-low heat conversion. *Nat Commun* 2015, 6:7915.
29. Plonska-Brzezinska ME. Carbon nanomaterials: perspective of their applications in biomedicine. *Curr Med Chem* 2019, 26:6832-3.
30. Jin L, Guo X, Gao D, Wu C, Hu B, Tan G, Du N, Cai X, Yang Z, Zhang X. NIR-responsive MXene nanobelts for wound healing. *NPG Asia Mater* 2021, 13:24.
31. Chung C, Kim Y-K, Shin D, Ryoo S-R, Hong BH, Min D-H. Biomedical applications of graphene and graphene oxide. *Acc Chem Res* 2013, 46:2211-24.
32. Sanles-Sobrido M, Rodríguez-Lorenzo L, Lorenzo-Abalde S, González-Fernández Á, Correa-Duarte MA, Alvarez-Puebla RA, Liz-Marzán LM. Label-free SERS detection of relevant bioanalytes on silver-coated carbon nanotubes: The case of cocaine. *Nanoscale* 2009, 1:153-8.
33. Fan Y, Cheng H, Zhou C, Xie X, Liu Y, Dai L, Zhang J, Qu L. Honeycomb architecture of carbon quantum dots: a new efficient substrate to support gold for stronger SERS. *Nanoscale* 2012, 4:1776-81.
34. Lee S, Hahm MG, Vajtai R, Hashim DP, Thurakitseree T, Chipara AC, Ajayan PM, Hafner JH. Utilizing 3D SERS active volumes in aligned carbon nanotube scaffold substrates. *Adv Mater* 2012, 24:5261-6.

35. Cheung W, Patel M, Ma Y, Chen Y, Xie Q, Lockard JV, Gao Y, He H.  $\pi$ -Plasmon absorption of carbon nanotubes for the selective and sensitive detection of  $\text{Fe}^{3+}$  ions. *Chem Sci* 2016, 7:5192-9.
36. Kramberger C, Hambach R, Giorgetti C, R ummeli MH, Knupfer M, Fink J, B uchner B, Reining L, Einarsson E, Maruyama S, Sottile F, Hannewald K, Olevano V, Marinopoulos AG, Pichler T. Linear Plasmon dispersion in single-wall carbon nanotubes and the collective excitation spectrum of graphene. *Phys Rev Lett* 2008, 100:196803.
37. Rana F. Graphene terahertz plasmon oscillators. *IEEE Trans Nanotechnol* 2008, 7:91-9.
38. Rodrigo D, Limaj O, Janner D, Etezadi D, Garc a de Abajo FJ, Pruneri V, Altug H. Mid-infrared plasmonic biosensing with graphene. *Science* 2015, 349:165-8.
39. Ponomarenko LA, Schedin F, Katsnelson MI, Yang R, Hill EW, Novoselov KS, Geim AK. Chaotic dirac billiard in graphene quantum dots. *Science* 2008, 320:356-8.
40. Bacon M, Bradley SJ, Nann T. Graphene quantum dots. *Part Part Syst Charact* 2014, 31:415-28.
41. Younis MR, He G, Lin J, Huang P. Recent advances on graphene quantum dots for bioimaging applications. *Front Chem* 2020, 8:424-49.
42. Thongrattanasiri S, Manjavacas A, Garc a de Abajo FJ. Quantum finite-size effects in graphene plasmons. *ACS Nano* 2012, 6:1766-75.
43. Lan C, Zhao J, Zhang L, Wen C, Huang Y, Zhao S. Self-assembled nanoporous graphene quantum dot- $\text{Mn}_3\text{O}_4$  nanocomposites for surface-enhanced Raman scattering based identification of cancer cells. *RSC Adv* 2017:18658-67.
44. Das R, Parveen S, Bora A, Giri PK. Origin of high photoluminescence yield and high SERS sensitivity of nitrogen-doped graphene quantum dots. *Carbon* 2020, 160:273-86.
45. Ebbesen TW. Carbon nanotubes. *Annu Rev Mater Sci* 1994, 24:235-64.
46. Wang D, Li Y, Li Puma G, Wang C, Wang P, Zhang W, Wang Q. Ag/AgCl@helical chiral  $\text{TiO}_2$  nanofibers as a visible-light driven plasmon photocatalyst. *Chem Commun* 2013, 49:10367-9.
47. Novoselov KS, Geim AK, Morozov SV, Jiang D, Zhang Y, Dubonos SV, Grigorieva IV, Firsov AA. Electric field effect in atomically thin carbon films. *Science* 2004, 306:666-9.
48. Ling X, Zhang J. First-layer effect in graphene-enhanced Raman scattering. *Small* 2010, 6:2020-5.
49. Zheng T, Feng E, Wang Z, Gong X, Tian Y. Mechanism of surface-enhanced Raman scattering based on 3D graphene- $\text{TiO}_2$  nanocomposites and application to real-time monitoring of telomerase activity in differentiation of stem cells. *ACS Appl Mater Interfaces* 2017, 9:36596-605.
50. Huang S, Pandey R, Barman I, Kong J, Dresselhaus M. Raman enhancement of blood constituent proteins using graphene. *ACS Photonics* 2018, 5:2978-82.
51. Qiu H, Wang M, Zhang L, Cao M, Ji Y, Kou S, Dou J, Sun X, Yang Z. Wrinkled 2H-phase  $\text{MoS}_2$  sheet decorated with graphene-microflowers for ultrasensitive molecular sensing by plasmon-free SERS enhancement. *Sens Actuators B Chem* 2020, 320:128445.
52. Dasgupta A, Rajukumar LP, Rotella C, Lei Y, Terrones M. Covalent three-dimensional networks of graphene and carbon nanotubes: synthesis and environmental applications. *Nano Today* 2017, 12:116-35.

53. Wang X, Shi W, Jin Z, Huang W, Lin J, Ma G, Li S, Guo L. Remarkable SERS activity observed from amorphous ZnO nanocages. *Angew Chem Int Ed* 2017, 56:9851-5.
54. Haldavnekar R, Venkatakrishnan K, Tan B. Non plasmonic semiconductor quantum SERS probe as a pathway for in vitro cancer detection. *Nat Commun* 2018, 9:3065.
55. Keshavarz M, Kassanos P, Tan B, Venkatakrishnan K. Metal-oxide surface-enhanced Raman biosensor template towards point-of-care EGFR detection and cancer diagnostics. *Nanoscale Horiz* 2020, 5:294-307.
56. Dharmalingam P, Venkatakrishnan K, Tan B. An atomic-defect enhanced Raman scattering (DERS) quantum probe for molecular level detection – Breaking the SERS barrier. *Appl Mater Today* 2019, 16:28-41.
57. Lin J, Ren W, Li A, Yao C, Chen T, Ma X, Wang X, Wu A. Crystal–amorphous core–shell structure synergistically enabling TiO<sub>2</sub> nanoparticles' remarkable SERS sensitivity for cancer cell imaging. *ACS Appl Mater Interfaces* 2020, 12:4204-11.
58. Qi D, Lu L, Wang L, Zhang J. Improved SERS sensitivity on plasmon-free TiO<sub>2</sub> photonic Mmicroarray by enhancing light-matter coupling. *J Am Chem Soc* 2014, 136:9886-9.
59. Liu B, Wang K, Gao B, Lu J, Li H, Zhao X. TiO<sub>2</sub>-coated silica photonic crystal capillaries for plasmon-free SERS analysis. *ACS Appl Nano Mater* 2019, 2:3177-86.
60. Lin J, Shang Y, Li X, Yu J, Wang X, Guo L. Ultrasensitive SERS detection by defect engineering on single Cu<sub>2</sub>O superstructure particle. *Adv Mater* 2017, 29:1604797.
61. Cong S, Yuan Y, Chen Z, Hou J, Yang M, Su Y, Zhang Y, Li L, Li Q, Geng F, Zhao Z. Noble metal-comparable SERS enhancement from semiconducting metal oxides by making oxygen vacancies. *Nat Commun* 2015, 6:7800.
62. Ermolaev GA, Stebunov YV, Vyshnevyy AA, Tatarkin DE, Yakubovsky DI, Novikov SM, Baranov DG, Shegai T, Nikitin AY, Arsenin AV, Volkov VS. Broadband optical properties of monolayer and bulk MoS<sub>2</sub>. *NPJ 2D Mater Appl* 2020, 4:21.
63. Donaldson K, Murphy FA, Duffin R, Poland CA. Asbestos, carbon nanotubes and the pleural mesothelium: a review of the hypothesis regarding the role of long fibre retention in the parietal pleura, inflammation and mesothelioma. *Part Fibre Toxicol* 2010, 7:5.
64. Song G, Gong W, Cong S, Zhao Z. Ultrathin two-dimensional nanostructures: surface defects for morphology-driven enhanced semiconductor SERS. *Angew Chem Int Ed* 2021, 60:5505-11.
65. Yang L, Qin X, Jiang X, Gong M, Yin D, Zhang Y, Zhao B. SERS investigation of ciprofloxacin drug molecules on TiO<sub>2</sub> nanoparticles. *Phys Chem Chem Phys* 2015, 17:17809-15.
66. Xue X, Ji W, Mao Z, Mao H, Wang Y, Wang X, Ruan W, Zhao B, Lombardi JR. Raman investigation of nanosized TiO<sub>2</sub>: effect of crystallite size and quantum confinement. *J Phys Chem C* 2012, 116:8792-7.
67. Xiong H-M, Xu Y, Ren Q-G, Xia Y-Y. Stable aqueous ZnO@polymer core–shell nanoparticles with tunable photoluminescence and their application in cell imaging. *J Am Chem Soc* 2008, 130:7522-3.

68. Zhao L-H, Zhang R, Zhang J, Sun S-Q. Synthesis and characterization of biocompatible ZnO nanoparticles. *CrystEngComm* 2012, 14:945-50.
69. Alessandri I. Enhancing Raman scattering without plasmons: unprecedented sensitivity achieved by TiO<sub>2</sub> shell-based resonators. *J Am Chem Soc* 2013, 135:5541-4.
70. Alessandri I, Depero LE. All-oxide Raman-active traps for light and matter: probing redox homeostasis model reactions in aqueous environment. *Small* 2014, 10:1294-8.
71. Bontempi N, Carletti L, De Angelis C, Alessandri I. Plasmon-free SERS detection of environmental CO<sub>2</sub> on TiO<sub>2</sub> surfaces. *Nanoscale* 2016, 8:3226-31.
72. Bontempi N, Biavardi E, Bordiga D, Candiani G, Alessandri I, Bergese P, Dalcanale E. Probing lysine mono-methylation in histone H3 tail peptides with an abiotic receptor coupled to a non-plasmonic resonator. *Nanoscale* 2017, 9:8639-46.
73. Lee N, Schuck PJ, Nico PS, Gilbert B. Surface enhanced Raman spectroscopy of organic molecules on magnetite (Fe<sub>3</sub>O<sub>4</sub>) nanoparticles. *J Phys Chem Lett* 2015, 6:970-4.
74. Li W, Zamani R, Rivera Gil P, Pelaz B, Ibáñez M, Cadavid D, Shavel A, Alvarez-Puebla RA, Parak WJ, Arbiol J, Cabot A. CuTe nanocrystals: shape and size control, plasmonic properties, and use as SERS probes and photothermal agents. *J Am Chem Soc* 2013, 135:7098-101.
75. Wang Y, Sun Z, Hu H, Jing S, Zhao B, Xu W, Zhao C, Lombardi JR. Raman scattering study of molecules adsorbed on ZnS nanocrystals. *J Raman Spectrosc* 2007, 38:34-8.
76. Zou Y, Jiang L, Zhai T, You T, Jing X, Liu R, Li F, Zhou W, Jin S. Surface-enhanced Raman scattering by hierarchical CuS microflowers: Charge transfer and electromagnetic enhancement. *J Alloys Compd* 2021, 865:158919.
77. Li S, Zhang H, Xu L, Chen M. Laser-induced construction of multi-branched CuS nanodendrites with excellent surface-enhanced Raman scattering spectroscopy in repeated applications. *Opt Express* 2017, 25:16204-13.
78. Syed H, Podagatlapalli GK, Mohiddon M, Soma VR. SERS studies of explosive molecules with diverse copper nanostructures fabricated using ultrafast laser ablation. *Adv Mater Lett* 2015, 6:1073-80.
79. Chen M, Li K, Luo Y, Shi J, Weng C, Gao L, Duan G. Improved SERS activity of non-stoichiometric copper sulfide nanostructures related to charge-transfer resonance. *Phys Chem Chem Phys* 2020, 22:5145-53.
80. Qiu Y, Lin M, Chen G, Fan C, Li M, Gu X, Cong S, Zhao Z, Fu L, Fang X, Xiao Z. Photodegradable CuS SERS probes for intraoperative residual tumor detection, ablation, and self-clearance. *ACS Appl Mater Interfaces* 2019, 11:23436-44.
81. Coleman JN, Lotya M, O'Neill A, Bergin SD, King PJ, Khan U, Young K, Gaucher A, De S, Smith RJ, Shvets IV, Arora SK, Stanton G, Kim H-Y, Lee K, Kim GT, Duesberg GS, Hallam T, Boland JJ, Wang JJ, Donegan JF, Grunlan JC, Moriarty G, Shmeliov A, Nicholls RJ, Perkins JM, Grievson EM, Theuwissen K, McComb DW, Nellist PD, Nicolosi V. Two-dimensional nanosheets produced by liquid exfoliation of layered materials. *Science* 2011, 331:568-71.

82. Ling X, Fang W, Lee Y-H, Araujo PT, Zhang X, Rodriguez-Nieva JF, Lin Y, Zhang J, Kong J, Dresselhaus MS. Raman enhancement effect on two-dimensional layered materials: graphene, h-BN and MoS<sub>2</sub>. *Nano Lett* 2014, 14:3033-40.
83. Muehlethaler C, Considine CR, Menon V, Lin W-C, Lee Y-H, Lombardi JR. Ultrahigh Raman enhancement on monolayer MoS<sub>2</sub>. *ACS Photonics* 2016, 3:1164-9.
84. Li Z, Jiang S, Xu S, Zhang C, Qiu H, Chen P, Gao S, Man B, Yang C, Liu M. Facile synthesis of large-area and highly crystalline WS<sub>2</sub> film on dielectric surfaces for SERS. *J Alloys Compd* 2016, 666:412-8.
85. Miao P, Qin J-K, Shen Y, Su H, Dai J, Song B, Du Y, Sun M, Zhang W, Wang H-L, Xu C-Y, Xu P. Unraveling the Raman enhancement mechanism on 1T' -Phase ReS<sub>2</sub> nanosheets. *Small* 2018, 14:1704079.
86. Lin J, Liang L, Ling X, Zhang S, Mao N, Zhang N, Sumpter BG, Meunier V, Tong L, Zhang J. Enhanced Raman scattering on in-plane anisotropic layered materials. *J Am Chem Soc* 2015, 137:15511-7.
87. Yin Y, Miao P, Zhang Y, Han J, Zhang X, Gong Y, Gu L, Xu C, Yao T, Xu P, Wang Y, Song B, Jin S. Significantly increased Raman enhancement on MoX<sub>2</sub> (X = S, Se) monolayers upon phase transition. *Adv Funct Mater* 2017, 27:1606694.
88. Sun L, Hu H, Zhan D, Yan J, Liu L, Teguh JS, Yeow EKL, Lee PS, Shen Z. Plasma modified MoS<sub>2</sub> nanoflakes for surface enhanced Raman scattering. *Small* 2014, 10:1090-5.
89. Li X, Guo S, Su J, Ren X, Fang Z. Efficient Raman enhancement in molybdenum disulfide by tuning the interlayer spacing. *ACS Appl Mater Interfaces* 2020, 12:28474-83.
90. Zheng Z, Cong S, Gong W, Xuan J, Li G, Lu W, Geng F, Zhao Z. Semiconductor SERS enhancement enabled by oxygen incorporation. *Nat Commun* 2017, 8:1993.
91. Liu Y, Gao Z, Chen M, Tan Y, Chen F. Enhanced Raman scattering of CuPc films on imperfect WSe<sub>2</sub> monolayer correlated to exciton and charge-transfer resonances. *Adv Funct Mater* 2018, 28:1805710.
92. Yin D, Wang M-L, Wang Y-Z, Hu X, Liu B, Liu H, Ma L, Gao G-G. A ternary ZnO/ZnS/MoS<sub>2</sub> composite as a reusable SERS substrate derived from the polyoxomolybdate/ZIF-8 host-guest framework. *J Mater Chem C* 2019, 7:9856-64.
93. Lv Q, Qin X, Lv R. Controllable growth of few-layer niobium disulfide by atmospheric pressure chemical vapor deposition for molecular sensing. *Front Mater* 2019, 6:279-88.
94. Lv Q, Wu X, Tan J, Liu B, Gan L, Li J, Huang Z-H, Kang F, Lv R. Ultrasensitive molecular sensing of few-layer niobium diselenide. *J Mater Chem A* 2021, 9:2725-33.
95. Song X, Wang Y, Zhao F, Li Q, Ta HQ, Rummeli MH, Tully CG, Li Z, Yin W-J, Yang L, Lee K-B, Yang J, Bozkurt I, Liu S, Zhang W, Chhowalla M. Plasmon-free surface-enhanced Raman spectroscopy using metallic 2D materials. *ACS Nano* 2019, 13:8312-9.
96. Kang SD, Snyder GJ. Charge-transport model for conducting polymers. *Nat Mater* 2017, 16:252-7.

97. Yuk H, Lu B, Lin S, Qu K, Xu J, Luo J, Zhao X. 3D printing of conducting polymers. *Nat Commun* 2020, 11:1604.
98. Das TK, Prusty S. Review on conducting polymers and their applications. *Polym Plast Technol Eng* 2012, 51:1487-500.
99. Yilmaz M, Babur E, Ozdemir M, Gieseck RL, Dede Y, Tamer U, Schatz GC, Facchetti A, Usta H, Demirel G. Nanostructured organic semiconductor films for molecular detection with surface-enhanced Raman spectroscopy. *Nat Mater* 2017, 16:918-24.
100. Lombardi JR. Enhanced by organic surfaces. *Nat Mater* 2017, 16:878-80.
101. Soluyanov AA, Gresch D, Wang Z, Wu Q, Troyer M, Dai X, Bernevig BA. Type-II weyl semimetals. *Nature* 2015, 527:495-8.
102. Qian X, Liu J, Fu L, Li J. Quantum spin hall effect in two-dimensional transition metal dichalcogenides. *Science* 2014, 346:1344-7.
103. Tao L, Chen K, Chen Z, Cong C, Qiu C, Chen J, Wang X, Chen H, Yu T, Xie W, Deng S, Xu J-B. 1T' Transition metal telluride atomic layers for plasmon-free SERS at femtomolar levels. *J Am Chem Soc* 2018, 140:8696-704.
104. Stock N, Biswas S. Synthesis of metal-organic frameworks (MOFs): routes to various MOF topologies, morphologies, and composites. *Chem Rev* 2012, 112:933-69.
105. Khan NA, Hasan Z, Jhung SH. Adsorptive removal of hazardous materials using metal-organic frameworks (MOFs): A review. *J Hazard Mater* 2013, 244-245:444-56.
106. García-García P, Müller M, Corma A. MOF catalysis in relation to their homogeneous counterparts and conventional solid catalysts. *Chem Sci* 2014, 5:2979-3007.
107. Fu J-H, Zhong Z, Xie D, Guo Y-J, Kong D-X, Zhao Z-X, Zhao Z-X, Li M. SERS-active MIL-100(Fe) sensory array for ultrasensitive and multiplex detection of VOCs. *Angew Chem Int Ed* 2020, 59:20489-98.
108. Powell JA, Venkatakrisnan K, Tan B. Toward universal SERS detection of disease signaling bioanalytes using 3D self-assembled nonplasmonic near-quantum-scale silicon probe. *ACS Appl Mater Interfaces* 2017, 9:40127-42.
109. Dougan JA, Faulds K. Surface enhanced Raman scattering for multiplexed detection. *Analyst* 2012, 137:545-54.
110. Grosset A-A, Dallaire F, Nguyen T, Birlea M, Wong J, Daoust F, Roy N, Kougioumoutzakakis A, Azzi F, Aubertin K. Identification of intraductal carcinoma of the prostate on tissue specimens using Raman micro-spectroscopy: A diagnostic accuracy case-control study with multicohort validation. *PLoS med* 2020, 17:e1003281.
111. Leong YX, Lee YH, Koh CSL, Phan-Quang GC, Han X, Phang IY, Ling XY. Surface-enhanced Raman scattering (SERS) taster: A machine-learning-driven multireceptor platform for multiplex profiling of wine flavors. *Nano Lett* 2021, 21:2642-9.
112. Mjejri I, Doherty CM, Rubio-Martinez M, Drisko GL, Rougier A. Double-sided electrochromic device based on metal-organic frameworks. *ACS Appl Mater Interfaces* 2017, 9:39930-4.

113. Naz S, Gul A, Zia M. Toxicity of copper oxide nanoparticles: a review study. *IET Nanobiotechnol* 2019, 14:1-13.
114. Kumar P, Gajbhiye K, Paknikar KM, Gajbhiye V. (2019) Current status and future challenges of various polymers as cancer therapeutic. In : *Polymeric nanoparticles as a promising tool for anti-cancer therapeutics*. (Ed. Kesharwani P, Paknikar KM, Gajbhiye V), 1-20. London: Elsevier.
115. Smolsky J, Kaur S, Hayashi C, Batra SK, Krasnoslobodtsev AV. Surface-enhanced Raman scattering-based immunoassay technologies for detection of disease biomarkers. *Biosensors* 2017, 7:7-28.
116. Zhao Z, Shen Y, Hu F, Min W. Applications of vibrational tags in biological imaging by Raman microscopy. *Analyst* 2017, 142:4018-29.
117. Lin-Vien D, Colthup NB, Fateley WG, Grasselli JG. (1991) The  $-C\equiv N$  and  $-N\equiv C$  groups. In: *The handbook of infrared and Raman characteristic frequencies of organic molecules*. (Ed. Lin-Vien D, Colthup NB, Fateley WG, Grasselli JG), 105-113. London: Academic Press.
118. Anbazhagan R, Vadivelmurugan A, Tsai H-C, Jeng R-J. Surface-enhanced Raman scattering of alkyne-conjugated  $MoS_2$ : A comparative study between metallic and semiconductor phases. *J Mater Chem C* 2018, 6:1071-82.
119. Mahouche-Chergui S, Gam-Derouich S, Mangeney C, Chehimi MM. Aryl diazonium salts: a new class of coupling agents for bonding polymers, biomacromolecules and nanoparticles to surfaces. *Chem Soc Rev* 2011, 40:4143-66.
120. Luo Y, Xiao Y, Onidas D, Iannazzo L, Ethève-Quellejeu M, Lamouri A, Félidj N, Mahouche-Chergui S, Brulé T, Gagey-Eilstein N, Gazeau F, Mangeney C. Raman reporters derived from aryl diazonium salts for SERS encoded-nanoparticles. *Chem Commun* 2020, 56:6822-5.
121. Li D, Luo Y, Onidas D, He L, Jin M, Gazeau F, Pinson J, Mangeney C. Surface functionalization of nanomaterials by aryl diazonium salts for biomedical sciences. *Adv Colloid Interface Sci* 2021, 294:102479.
122. Zong Y, Hu J, Wang Y, Sun H, Li Y, Liu W. Blank experimental study on the determination of nitrogen and oxygen isotopes by chemical conversion method. *RSC Adv* 2019, 9:37267-73.